Movement-informed projections of Bristol Bay red king crab seasonal distribution to support spatial management decisions

Sean B. Hardison[1,2*], Erin J. Fedewa[2], Leah Zacher[2], James T. Thorson[3], Emily R. Ryznar[2], Kelly A. Kearney[3], Shannon M. Hennessey[2], Benjamin J. Daly[4], Scott Goodman[5], Michael A. Litzow[2], Franz Mueter[1]

[1]College of Fisheries and Ocean Sciences, University of Alaska Fairbanks, 17101 Point Lena Loop Rd., Juneau, AK, 99801

[2]Shellfish Assessment Program, Alaska Fisheries Science Center, National Marine Fisheries Service, NOAA, 301 Research Ct, Kodiak, AK 99615

[3]Resource Ecology and Fisheries Management Division, Alaska Fisheries Science Center, National Marine Fisheries Service, NOAA, 7600 Sand Point Way N.E., Seattle, WA 98115

[4]Division of Commercial Fisheries, Alaska Department of Fish and Game, 351 Research Ct, Kodiak, AK 99615

[5]Bering Sea Fisheries Research Foundation, 4039 21st Ave West, Ste 404, Seattle, WA 98199

*Corresponding author: sbhardison@alaska.edu

Abstract

Understanding seasonal shifts in the spatial distribution of Bristol Bay red king crab (BBRKC) is essential to developing adaptive management strategies that promote sustainable harvest. Although fishery harvests suggest a substantial shift in the distribution of male crab between late spring (when fishery-independent bottom trawl surveys occur) and autumn (during the directed fishery), the environmental drivers underlying this shift are not well characterized. In this study, we fit an advection-diffusion model of mature male BBRKC seasonal movements to pop-up satellite archival tag data to estimate the habitat preferences of migrating crab. We then used estimated habitat preference parameters and time-varying environmental data to project the distribution of the BBRKC stock from the late spring to the autumn during 2005-2023, evaluating the similarities between these projected distributions and directed fishery catches through spatial overlap analysis. Our habitat preference model suggested that late spring to autumn mature male BBRKC movements were explained by a preference for cooler temperatures in central Bristol Bay in October, with preference for shallow habitats at low tidal current velocities and deeper habitats at higher velocities. We found that projections of seasonal BBRKC distributions estimated from the movement model skillfully predicted interannual variation in directed BBRKC fishery catches. Our results offer new insights into the environmental drivers of seasonal BBRKC movements and demonstrate the utility of movement-integrated species distribution modeling for seasonal projections of animal distributions.

Keywords: *red king crab, Bristol Bay, habitat preference, spatiotemporal model, spatial overlap, Pop-up satellite archival tag, animal movement, advection-diffusion model*

Introduction

The Bristol Bay red king crab (BBRKC; *Paralithodes camtschaticus*) fishery was once one of the most productive crab fisheries in the world. The fishery peaked in 1980 when 58,943 tons of crab worth an estimated $115.3 million ex-vessel value were harvested, but had collapsed by 1982 when the fishery landed only 1,361 tons of crab (Zheng and Siddeek 2018, Palof 2024). After moderate recovery and then additional stock decline in the mid-1990s, managers implemented trawl closure areas in 1995 and 1996, including the Red King Crab Savings Area (RKCSA) and Nearshore Bristol Bay Trawl Closure Area (NBBTCA). These closure areas were designed to protect BBRKC by limiting negative interactions with trawl fisheries, and together closed ~79,000 km^2 of BBRKC habitat to trawling (Kruse et al. 2010). However, evaluating the efficacy of these closure areas and ensuring their future utility amidst increasingly anomalous environmental conditions in the Bering Sea (Stabeno and Bell 2019, Litzow et al. 2024) and climate-driven shifts in species distributions (Szuwalski et al. 2021, Howard et al. 2024) requires improved knowledge of BBRKC habitat preferences, seasonal migrations and distributions. Developing this understanding has the potential to inform new management strategies (e.g., spatially dynamic closure areas) that optimize for the diverse economic and ecological sustainability objectives of stakeholders (Hazen et al. 2018) in Bristol Bay.

Our current understanding of seasonal red king crab migrations and distributions stems from decades of tagging studies (Powell and Reynolds 1965, Takeshita et al. 1990, Stone et al. 1992), bottom trawl and pot surveys (Dew 2008, Loher et al. 2024, Zacher et al. 2024), directed fishery harvest reports (Zacher et al. 2018, Ryznar et al., *in review*), and bycatch observations from groundfish fisheries (Ryznar and Litzow 2024) in Bristol Bay and elsewhere in Alaskan waters. However, a lack of standardized sampling methods among seasons complicates inferring migratory patterns and behaviors from these sources. Additionally, when predictions of seasonal distribution are possible, for example, within bycatch distribution modeling frameworks, model training data are spatially restricted to regions where groundfish fisheries operate and do not include critical crab habitats in the RKCSA or NBBTCA that are closed to

72 trawling (Laman et al. 2018, Ryznar and Litzow 2024). The quality of our understanding of BBRKC
73 seasonal distributions is therefore weighted towards the late spring, when a spatially-comprehensive
74 fisheries-independent bottom trawl survey occurs, and the autumn, when the directed BBRKC fishery
75 operates in Bristol Bay. Extending our knowledge of BBRKC distribution outside the late spring and
76 autumn periods to better characterize the efficacy of BBRKC trawl closure areas requires methods that
77 can produce robust predictions of stock distribution by integrating across seasons and disparate sampling
78 methodologies (e.g., telemetry data via satellite tags, bottom trawl and pot surveys, observations of
79 BBRKC bycatch, and/or directed fishery harvest data).
80 "Hybrid" species distribution models (SDMs) are one method to address this challenge (Thorson
81 et al. 2021, Thorson and Kristensen 2024). The hybrid SDM framework functions by extending spatially-
82 resolved predictions of animal distribution, made using a correlational SDM (e.g., a generalized linear
83 mixed model or machine learning model) fitted to observations of presence/absence or density in relation
84 to environmental covariates (Dormann et al. 2012), over a time interval by coupling distributional
85 predictions with movement probabilities over that time interval (Thorson et al. 2021). Movement
86 probabilities are calculated using a model fitted to telemetry data estimating the contributions to observed
87 animal movement by taxis, (i.e., the directional movement of individuals towards preferred habitats), and
88 diffusion (i.e., the residual, non-directional movement not captured by taxis) (Thorson and Kristensen
89 2024). Ultimately, the coupling of predicted distributions from a SDM with predicted movement
90 probabilities from a movement model produces distributional projections consistent with the habitat
91 preferences of tagged individuals, where habitat preference refers to the use of a particular habitat relative
92 to its availability (Aarts et al. 2008).
93 Two key environmental factors contributing to the habitat preferences of seasonally migratory red
94 king crab include depth (Wallace et al. 1949, Powell and Reynolds 1965, Stone et al. 1992) and bottom
95 temperatures (Loher and Armstong 2005, Chilton et al. 2010, Zacher et al. 2018). During the winter-
96 spring period, mature female BBRKC move into shallow, nearshore habitats where annual molting and

mating occurs (Dew 2008, Chilton et al. 2010). A subset of the male population, typically the large, old-shell individuals, concurrently migrates into shallow habitats to participate in mating (Dew 2008), whereas smaller, recently molted males remain in deeper habitats (Takeshita et al. 1990, Dew and McConnaughey 2005). Following the molt-mate phase, both male and female crab migrate back to deeper habitat (Dew 2008, Chilton et al. 2010), with post-spawning males and females tending to segregate spatially, and recently-mated old-shell males reconvening with the population of new-shell males (Takeshita et al. 1990). The female molt-mate cycle may be delayed in colder bottom temperature years, resulting in the shallow-to-deep, post-spawning migration of mature female crab occurring as late as July (Chilton et al. 2010).

For legal male BBRKC (≥ 135 mm carapace length [CL]), migratory dynamics between the summer and autumn months are evidenced by data collected by the National Marine Fisheries Service eastern Bering Sea (NMFS EBS) bottom trawl survey that begins in Bristol Bay in late May-early June (Zacher et al. 2024), and spatially-resolved catch data provided by vessel captains and observers in the male-only directed fishery open between October 15 and January 15 annually (the majority of landings in the directed fishery occur within the first month; Zacher et al. 2018). Although observations from the directed fishery only occur within a portion of the range occupied by BBRKC, comparison of stock distribution between the two seasons reveals a general distributional shift from central Bristol Bay in the late spring to the south and/or west when crab are captured in the fishery (Zacher et al. 2018). In general, the spatial distribution of the stock during the directed fishery tends to be deeper than during the survey in late spring, and harvests in colder bottom temperature years tend to arrange in a band-like formation along the Alaska Peninsula, whereas in warmer years, harvests tend to extend further northwards into central Bristol Bay (Zacher et al. 2018). In recent years, satellite tags have been deployed on crab during the NMFS EBS survey to better understand the seasonal movements of mature/legal male crab (≥ 120 mm CL) (NPFMC 2022a-c, 2024a, Nault et al. 2024).

The availability of observations of BBRKC density from a fisheries-independent bottom trawl survey that occurs annually during the late spring, coupled with observations of BBRKC movement over the late spring–autumn interval, presents a unique opportunity to evaluate the utility of a hybrid SDM applied to the BBRKC stock. In this work, we applied the hybrid SDM framework to 1) estimate mature male BBRKC habitat preferences based on relationships between environmental variables and BBRKC movements, and 2) integrate BBRKC late spring survey data, tagging data, and habitat preferences to project BBRKC density across the late spring–autumn period. We evaluated the predictive skill of our projections by comparing the spatial overlap of projected BBRKC distributions with the distribution of autumn BBRKC fishery catches for each year between 2005 and 2023. We expected that the spatial overlap between projected and fishery distributions would be greater than what would be expected if crab moved randomly over the late spring–autumn periods. Lastly, we considered how bottom temperatures in Bristol Bay influenced the extent of spatial overlap and trends in stock distribution.

Methods

Overview of the hybrid modeling approach

We applied a two-stage hybrid modeling approach to project BBRKC density (numbers km^{-2}) from late spring (June) to autumn (October). This two-stage approach to projecting density specifically involved the integration of predictions from two separate models, rather than generating predictions from a single, jointly estimated model (Thorson et al. 2021, Thorson and Kristensen 2024). We first fitted a spatial generalized linear mixed model, hereafter the species distribution model (SDM), to BBRKC densities from the NMFS EBS bottom trawl survey to predict June BBRKC density and distribution. Next, we fitted a model of crab seasonal movements, hereafter the diffusion-taxis model (Thorson et al. 2021, Thorson and Kristensen 2024), to telemetry data (the known tag release and recovery locations) to predict BBRKC movements from June to October. The diffusion-taxis model estimated movement due to

144 taxis, or the directed movement of individuals towards preferred habitats, and diffusion, or the non-
145 directed movement of individuals over the time interval (Thorson and Kristensen 2024). Contributions of
146 "drift", or the passive, directional movement of animals; for example, due to currents, may also be
147 estimated but were not considered in our analyses. We assumed that the movements of these large-bodied
148 benthic crustaceans would be primarily driven by taxis rather than by passive movement in response to
149 current dynamics.

150 We then multiplied June density predictions from the SDM with predicted movement
151 probabilities from the diffusion-taxis model to project BBRKC density across the June–October interval.
152 We used AIC (Akaike 1987) and leave-one-out cross validation (LOOCV) to identify the best-fitting
153 model with highest prediction skill among a set of uniquely parameterized diffusion-taxis models. After
154 model selection, we used a parametric bootstrap approach to evaluate the skill of annual BBRKC density
155 projections made using the selected diffusion-taxis model relative to a diffusion-only model. Specifically,
156 we compared the extent of spatial overlap between density projections made using the diffusion-taxis
157 model or diffusion-only model with catch per unit effort (CPUE) from the directed BBRKC fishery.

158 Survey data

159 We used data collected on the 2005-2019 and 2021-2023 NMFS EBS bottom trawl surveys to fit
160 SDMs. We chose the 2005 start year for this analysis because 2005 was the first year for which spatially-
161 resolved commercial harvest data from the BBRKC directed fishery were available. The NMFS EBS
162 bottom trawl survey follows a fixed station sampling design with survey stations spaced 20 nautical miles
163 apart. Thirty-minute trawls were conducted using an 83-112 eastern otter trawl with 25.3 m headrope and
164 34.1 m footrope (see full trawl specifications in Markowitz et al. 2023). The survey typically begins in
165 late May at stations in eastern Bristol Bay, moving westward and out of Bristol Bay by late June. Station-
166 level mature male BBRKC density was estimated as the total number of mature males caught divided by
167 area-swept effort (catch per unit effort; crab km^{-2}).

Tagging data

Hardshell mature male red king crab (carapace length [CL] between 124 and 183 mm) were tagged during the EBS bottom trawl survey between May 29 and June 22 in 2021-2023 (Table 1). Crab brought up in good condition in trawl nets were candidates for tagging, and all individuals tagged had walking legs intact and very minor to no injuries evident. To the extent practical while on a survey vessel, the distribution of released tags was weighted by the density of BBRKC survey catches within a given survey year, such that more tags were released in areas with higher densities of BBRKC from survey catches. Crab were tagged with PSAT tags from Wildlife Computers (miniPAT and Mark Report PAT; Table 1) by securing the tag to a polyolefin tubing harness wrapped around the crab's carapace (see Nault et al. 2024). The positively buoyant tags float approximately 7 cm above the tagged crabs. This attachment method does not allow tags to be retained through the molt, but male BBRKC do not generally molt during the deployment period (NPFMC 2024b).

Data from 2020 were available for use in this study (Nault et al. 2024), but were not included in our models due to temporal and spatial differences in tag deployment methods between the 2020 and 2021-2023 tagging studies. In 2020, the median tag deployment date of July 7th came over a month later than 2021-2023 tags (2021: June 6th, 2022: June 5th, 2023: June 2nd), and tags were deployed in clusters in 2020 rather than as in 2021-2023 where tag deployment density was weighted by survey BBRKC catch density. We programmed tags to release from crab between October 11th and 13th (Table 1). Once at the surface, satellite tags drifted for 0.1 to 48 hours prior to an initial high-quality Argos location estimate. To correct for tag surface drift we estimated true pop-up locations and error ellipses using known tag drift vectors (Nault et al. 2024). Tags that surfaced before the programmed release date, most likely due to crab death, were not included in this analysis. Across the three-year tagging period, June deployment and October pop-up locations were obtained for 63 mature male BBRKC (Table 1). PSAT tags yielded positional information for crabs at tag deployment (June) and pop-up (October) locations.

Commercial fishing data

We used spatially-resolved daily fishing logbook data collected by BBRKC commercial fishing boat captains to calculate CPUE and to evaluate the overlap between the spatial distribution of fishery CPUE and projected BBRKC distributions. Daily fishing logbook observations, which include catch size and location, have been kept by BBRKC fishery captains since the rationalization of the fleet in 2005. BBRKC are fished using large rectangular mesh pots (e.g., $7' \times 7' \times 4'$) that are set in groups along straight lines referred to as "strings" with on average 23 pots per string. Each daily fishing log entry detailing catch size refers to the number of legal sized male crabs harvested along the entire string, and we calculated CPUE as the number of crabs harvested per string divided by the number of pots hauled following Zacher et al. 2018. Strings with ≥ 100 and < 5 pots were omitted from CPUE calculations, as very long strings were unlikely to be set in straight lines or well-described by the unique coordinate pair that we assigned to each string, and strings with very few pots were removed due to low sample size. Fishing boat captains record the coordinates of the start and end pot for each string, and in our analyses, we assigned string position as the average of these coordinates.

Species distribution model

We fitted a spatial generalized linear mixed model to observations of BBRKC density with spatial and spatiotemporal random fields, Tweedie observation error and log link (Anderson et al. 2024). We included survey year as a categorical predictor estimated as a fixed effect. The model was given by

$$\mathbb{E}[r_{\boldsymbol{s},y}] = \mu_{\boldsymbol{s},y}$$

$$\mu_{\boldsymbol{s},y} = \exp(\alpha_y + \omega_{\boldsymbol{s}} + \epsilon_{\boldsymbol{s},y}) \quad (1)$$

$$\boldsymbol{\omega} \sim \text{MVN}(\mathbf{0}, \boldsymbol{\Sigma}_{\omega})$$
$$\boldsymbol{\epsilon_y} \sim \text{MVN}(\mathbf{0}, \boldsymbol{\Sigma}_{\epsilon}),$$

where $r_{\boldsymbol{s},y}$ is the observed density of mature male crab at survey station $\boldsymbol{s}$ in year y, $\mu_{\boldsymbol{s},y}$ is the predicted density, α_y is an estimated intercept for each year, $\boldsymbol{\omega}$ is the main effect for space and represents a

temporally-persistent deviation in log-density at location *s*, and $\boldsymbol{\epsilon_y}$ is the interaction of space and year that is estimated independently for each year. Both spatial and spatiotemporal random fields were treated as Gaussian Markov random fields with the Stochastic Partial Differential Equation (SPDE) method (Lindgren et al. 2011), and spatial covariances for matrices $\boldsymbol{\Sigma}_\omega$ and $\boldsymbol{\Sigma}_\epsilon$ were calculated using a Matérn covariance function (Cressie and Huang 1999). We used a SPDE mesh with 470 vertices where the maximum distance between vertices within the study area was 25 km (Appendix S1: Fig. S1a).

We fitted the SDM to survey data between 2005 and 2023 (excluding 2020 when no bottom trawl survey occurred due to COVID-19) using the R package *sdmTMB* (Anderson et al. 2024). We used this model to predict June BBRKC densities during these years across *J* grid cells (grid cell area = 625 km^2); resulting in the yearly density vector $\boldsymbol{c_y}$ with *J* elements. The prediction grid (Appendix S1: Fig. S1b, purple) was a subset of the Bristol Bay RKC management district (54.5-58.5°N, 168-158°W) that we extended to include a region in northwest Bristol Bay where satellite tags were deployed on RKC. This extension was immediately adjacent to the northern management boundary and extended to 59.1°N, 166.2°W (see tags deployed outside Bristol Bay management district in Fig. 1). We limited the extent of the prediction grid in southwest Bristol Bay to avoid projecting BBRKC density far outside the region within which crab movement data were available. Between 99.6% and 100% of annual fishing CPUE observations fell within this prediction grid during the study period.

Diffusion-taxis model

Next, we fitted a diffusion-taxis model to BBRKC tagging data to predict the probabilities of crab moving from one grid cell to any other grid cell within the prediction grid over the June-October time interval (Thorson et al. 2021, Thorson and Kristensen 2024). Positional information from PSAT tags was available for start (June) and end (October) positions of tagged crabs. We used a spatial grid comprised of $J = 296$ grid cells to define adjacency matrix $\mathbf{A}$ with dimension $J \times J$ (Appendix S1: Fig. S1b, black). We used this grid that had fewer cells than the prediction grid (296 vs. 313) to reduce the computational

complexity of likelihood optimization and aid in model convergence. The larger 313 cell grid was used for prediction as this grid more accurately captured the spatial boundaries of the Bristol Bay management district. Values of **A** were 1 when cells shared sides and 0 otherwise (i.e., rook adjacency). Given tagging observations from multiple years, we calculated the year-specific instantaneous movement rate matrix $\dot{\mathbf{M}}_y$ for crab moving between adjacent cells per unit time *t* as a combination of diffusion and taxis that were estimated from tagging data. $\dot{\mathbf{M}}_y$ had the same sparsity structure as **A,** such that crab could only move to adjacent cells in instantaneous time. In the diffusion-taxis model, $\dot{\mathbf{M}}_y$ is the sum of instantaneous diffusion $\dot{\mathbf{D}}_y$ and taxis $\dot{\mathbf{Z}}_y$ rates:

$$\dot{\mathbf{M}}_y = \dot{\mathbf{D}}_y + \dot{\mathbf{Z}}_y \tag{2}$$

Here, diffusion $\dot{\mathbf{D}}_y$ is defined as random, isotropic (i.e., non-directional) movement and taxis $\dot{\mathbf{Z}}_y$ as active directional movement in response to habitat preferences. Elements of $\dot{\mathbf{D}}_y$ and $\dot{\mathbf{Z}}_y$ matrices are $\dot{d}_{y,g_1,g_2}$ and $\dot{z}_{y,g_1,g_2}$, respectively, reflecting the movement rates of crab due to diffusion and taxis from g_1 to adjacent grid cell g_2 per unit time. The diffusion rate $\dot{d}_{y,g_1,g_2}$ is given by

$$\dot{d}_{y,g_1,g_2} = \begin{cases} D\frac{1}{\Delta_s^2}a_{g_1,g_2} & \text{if } g_1 \neq g_2 \\ -\sum_{g\neq g_2}\dot{d}_{y,g_1,g} & \text{if } g_1 = g_2 \end{cases}, \tag{3}$$

where D is the diffusion coefficient estimated from tagging data in units distance^2/time, Δ_s^2 is the grid cell area with sides of length Δ_s, and a_{g_1,g_2} is the corresponding element of the adjacency matrix.

For taxis between cells g_1 and g_2, the taxis rate $\dot{z}_{y,g_1,g_2}$ is

$$\dot{z}_{y,g_1,g_2} = \begin{cases} (h_{y,g_1} - h_{y,g_2})\frac{1}{\Delta_s}a_{g_1,g_2} & \text{if } g_1 \neq g_2 \\ -\sum_{g\neq g_2}\dot{z}_{y,g_1,g} & \text{if } g_1 = g_2 \end{cases}, \tag{4}$$

where $h_{y,g}$ is habitat preference modeled as

$$h_{y,g} = \boldsymbol{x}_{y,g}\boldsymbol{\theta} + \boldsymbol{w}_{y,g}\boldsymbol{\lambda}, \tag{5}$$

and where **X** indicates the four basis functions for representing a cubic thin plate spline of bottom temperature, $\boldsymbol{x}_{y,g}$ are their values for year *y* and location *g*, such that $\boldsymbol{\theta}$ is a vector of estimated parameters

representing the response to bottom temperature. Similarly, **W** indicates the nine basis functions derived from a cubic regression tensor spline of depth and current velocity, $\boldsymbol{w}_{y,g}$ are their specific values, and where $\boldsymbol{\lambda}$ is the vector of parameters representing the interaction of these two covariates. The provenance of environmental covariates included in the habitat preference model is described below. Given parameters D, $\boldsymbol{\theta}$ and $\boldsymbol{\lambda}$ in the diffusion-taxis model, we calculated the instantaneous movement rate $\dot{\mathbf{M}}_y$. We then calculated the integrated movement fraction over the typical 19 week tag deployment interval Δ_t as $\mathbf{M}_y = \exp(\Delta_t \dot{\mathbf{M}}_y)$. Although there were differences in tag deployment date within years due to survey timing (Table 1), we assumed that tags were deployed on June 5th (median tag deployment date) and popped up on October 13th (median tag pop-up date), which yielded the 19-week interval. Given a release in year y and location g_1, the probability $\pi_{y,g}$ of ending up in cell g is therefore the vector obtained when extracting row g_1 from matrix $\mathbf{M}_y$. We then calculated the joint log-likelihood by summing $\log(\pi_{y,g})$ across all years and tags. We estimated model parameters by finding the parameter values that maximized this log-likelihood of observing crab movement between tag deployment and pop-up locations over Δ_t.

We evaluated bottom temperature ("*temp*"), depth, and maximum tidal current ("*velocity*") for inclusion in the habitat preference model (Table 2), given that these covariates have been shown to be important for predicting BBRKC fishery harvest distributions (Ryznar and Litzow, *in review*). Due to limited tagging observations that precluded us from fitting habitat preference curves for each year, we assumed that movement parameters (D, $\boldsymbol{\theta}$ and $\boldsymbol{\lambda}$) were constant across years. For our temperature covariate, we used the bottom temperature output from reanalysis-driven hindcast simulations of the northeast Pacific regional implementation of the Modular Ocean Model version 6 (MOM6–NEP10k) that has been shown to skillfully predict Bering Sea bottom temperatures (Drenkard et al. 2024, Seelanki et al. 2025). We retrieved daily bottom temperature data from October 8 to 13 for each year in 2005–2019 and 2021–2023, then averaged each year's data to create annual bottom temperature spatial layers. We also included bottom depths sourced from the General Bathymetric Chart of the Oceans (GEBCO 2023) and maximum tidal current velocities across Bristol Bay over the 1 January 2009-4 January 2010 period

(Egbert and Erofeeva 2002, Laman et al. 2018) as static covariates. This latter covariate has been used in the spatial modeling of essential fish habitat in the Eastern Bering Sea in recent years (Laman et al. 2022). All spatial layers were averaged to the 625 km^2 spatial resolution to match that of the prediction grid. We performed spline basis expansion using the *mgcv* R package (Wood 2006) and fitted the preference model using maximum likelihood estimation in R with RTMB (v4.4.1; R Core Team 2024, Kristensen 2024). We did not penalize basis parameters during model estimation like is done natively in the *mgcv* R package (Wood 2006).

We used AIC to select the most parsimonious habitat preference model from a set of six candidate models (Table 2). The selection set included 1) the diffusion-only model with no habitat preference components specified, 2) a model treating the three habitat covariates as linear predictors of habitat preference and 3) a model treating the three habitat covariates as univariate smooth functions of habitat preference using thin-plate regression splines. Models 4–6 each used a cubic regression tensor spline to capture the interaction between two habitat covariates and a separate univariate smooth for the third, differing in the covariates included in the tensor interaction and univariate smooth terms.

Seasonal projections

We combined predictions from the SDM and movement probabilities from the selected diffusion-taxis model to make seasonal projections of BBRKC distributions into October when tags popped up. Given the year-specific vector of predicted late spring crab densities $\boldsymbol{c}_y$ from the SDM and estimated movement fraction matrix $\mathbf{M}_y$ from the diffusion-taxis model, the vector of projected October crab densities $\boldsymbol{c}_{y,t+\Delta_t}$ was

$$\boldsymbol{c}_{y,t+\Delta_t}^T = \boldsymbol{c}_{y,t}^T \mathbf{M}_y. \quad (6)$$

We used this approach to project October crab densities for each year between 2005 and 2023 where summer survey data were available.

Overlap between projected BBRKC densities and directed fishery harvests

To evaluate the predictive skill of the modeled distributions relative to fishery dependent data, we compared projected BBRKC densities to observed catch patterns from the fishery, recognizing that fishery CPUE reflects both biological (e.g., crab density) and fishery-driven processes (e.g., the spatial distribution of effort may either be associated with areas where captains have had success in previous seasons or be constrained by costs to access). We calculated the extent of overlap between projected October BBRKC density and CPUE from the directed BBRKC fishery (October 15 season opening) for each year between 2005 and 2023 (excluding 2020-2022 when either no bottom trawl survey or fishery occurred) using Bhattacharyya's coefficient (Bhattacharyya 1943). Bhattacharyya's coefficient can be interpreted as the degree of similarity between two populations in their use of space (Carroll et al. 2019). Bhattacharyya's coefficient for year y (B_y) is calculated as

$$B_y = \sum_{g=1}^{J} \sqrt{P_{proj_{y,g}} \times P_{catch_{y,g}}}, \quad (7)$$

where $P_{proj_{y,g}}$ and $P_{catch_{y,g}}$ are year-specific proportions of total projected BBRKC densities and average BBRKC fishery CPUE within a given grid cell g. This method provides an intuitive approach to estimating the extent of spatial overlap because B_y ranges from 0 in the case of no overlap to 1 when relative population densities are identical; that is, $P_{proj_{y,g}} = P_{catch_{y,g}}$ for all g (Fieberg and Kochanny 2005).

Evaluating movement model and movement-informed projection skill

We used leave-one-out cross-validation (LOOCV) to evaluate movement model prediction skill for years when tags were available (2021-2023). The LOOCV analysis involved fitting the six movement models (Table 2) 63 times (the total number of tags) with a different tagging observation dropped from the training data during each training iteration. We then predicted the pop-up location of the tag that was excluded from the training set and calculated the distance between the predicted and observed pop-up

location, yielding 63 distance residuals that we used to calculate root mean squared error (RMSE) as our measure of prediction skill. Predicted tag pop-up locations were the positions given by the weighted average of longitudes and latitudes of grid cell centroids where weights were grid cell movement fractions. We used RMSE calculated from this LOOCV analysis to quantify the prediction skill of movement models, and used this metric in addition to AIC to select the best-fitting model for use in projection analyses.

We used a parametric bootstrap analysis to evaluate the predictive skill of movement-informed density projections in years when bottom trawl survey and fishery CPUE data were available (2005-2019, 2023). For each year, we took N = 1000 draws from a 1) multivariate normal distribution with mean and covariance specified by the estimated parameters and covariances in the fitted diffusion-taxis model, and 2) a normal distribution with mean and variance specified by the estimated diffusion parameter mean and variance in the diffusion-only model. This diffusion-only model represented movement due to random, non-directional movement alone, and therefore served as a null model for comparison with outcomes from the diffusion-taxis model. The diffusion-taxis model from which parameter samples were drawn used the AIC/RMSE-selected habitat preference model (Eq. 5) that included interannually varying hindcasts of bottom temperature from MOM6 during the October 8–13 period as a covariate. Additionally, for all years where SDM predictions were available, we simulated draws from the precision matrix of the fitted SDM and used the simulated parameters to predict the distribution of BBRKC during June (N = 1000 per year).

For all years where SDM predictions were available and the BBRKC fishery was open (2005-2019; 2023), we combined the simulated June BBRKC distribution with the simulated parameters from the diffusion-taxis and diffusion-only models to project BBRKC density into October of that year (Eq. 6). This produced two sets of simulated projections, one reflecting projections made using the diffusion-taxis model, and the other reflecting projections made using the diffusion-only model. We calculated Bhattacharyya's coefficient (B) for each projection to quantify the spatial overlap between projected

October BBRKC densities and fishery catches that we assumed to be known without error. Additionally, we calculated the annual centroids for projected October BBRKC density using the diffusion-taxis and diffusion-only models for comparison with the centroid of BBRKC fishery catches, where centroids were the coordinates specified by the projected density- or CPUE-weighted average longitude and latitude. We then calculated the distance between fishery CPUE centroids and projected density centroids using the diffusion-taxis and diffusion-only models.

We calculated bootstrap-based means and 95% confidence intervals for 1) the paired difference between spatial overlap (B) calculated from diffusion-taxis model- and diffusion-only model-informed projections (2005-2019; 2023), and 2) the distance between fishery and projected density centroids derived from the diffusion-taxis model and diffusion-only model (2005-2019; 2023). We also calculated bootstrap P values for testing the hypotheses that 1) the paired difference between spatial overlap (B) calculated from diffusion-taxis model- and diffusion-only model-informed projections was greater than 0, and 2) the distance between fishery and projected density centroids was smaller when projections were made using the diffusion-taxis model compared to the diffusion-only model ($\alpha = 0.05$).

Effects of bottom temperature on spatial overlap and BBRKC distribution

We also tested the hypothesis that the difference in spatial overlap using either diffusion-taxis model- or diffusion-only–based projections (B_{DTM}–$B_{\mathrm{diff.\ only}}$) was a function of bottom temperature by modeling B_{DTM}–$B_{\mathrm{diff.\ only}}$ as a smooth function of bottom temperature with a thin plate spline with three basis dimensions. We evaluated the relationships between the longitude and latitude components of diffusion-taxis model-based projection centroids and those derived from directed fishery CPUE using linear regression. Lastly, we visualized the position of fishery CPUE and diffusion-taxis model projections of BBRKC density centroids relative to bottom temperature conditions in Bristol Bay. To do this, we averaged MOM6 bottom temperature outputs over the prediction grid for October 8-13 annually for all years between 2005 and 2023.

Results

BBRKC movement patterns

Over the June-October study period, the average distance between tag release and pop-up location was 100 +/- 50 km (mean +/- sd), and tagged BBRKC moved on average 0.8 +/- 0.4 km day^{-1}. The largest distance between tag release and pop-up was 225 km, and the smallest was 6 km. In units of degrees clockwise from North, the average direction of movement across all tags was 220 +/- 40°, indicating that crab typically traveled southwest from tag release locations (270° would be due west and 180° due south; Fig. 1). Of the 31 tags that were released in the Nearshore Bristol Bay Trawl Closure Area (NBBTCA) or the Red King Crab Savings Area (RKCSA), 100% of tags popped-up in those areas, and 61% (19/31) of tags released in those areas popped-up specifically in the RKCSA. The average direction of movement and distance traveled for tags released in closure areas was 240 +/- 40° (roughly southwest on average) and 100 +/- 60 km, respectively. Of the 17 tags released to the east of 164°W but not within a closure area (the western boundary of the RKCSA is 164°W), 88% of tags popped up within a closure area (15/17), such that 96% of tags released east of 164°W popped up in a closure area. There were 15 tags released west of 164°W and none of those tags popped-up in a closure area. The average direction of movement and distance traveled for individuals tagged west of 164°W was 220 +/- 40° (roughly south-southwest on average) and 90 +/- 40 km, respectively. Neither the average direction of tag movement nor the distance traveled significantly differed between tags released west and east of 164°W.

However, tags released east of 164°W popped up in habitats that were significantly deeper than those tags released west of 164°W (t.test, $t = 7.4$, df = 19.1, $P < 0.001$); tags released east of 164°W (the vast majority of which moved into closure areas) popped up in habitats with an average depth of 74 +/- 6 m, and tags released west of 164°W popped up in habitats with an average depth of 56 m +/- 8 m. Tags released east of 164°W also popped up in habitats exposed to greater maximum tidal currents compared to those released west of 164°W ($t = 15.8$, df = 24.9, $P < 0.001$). The mean maximum tidal current

velocity in pop-up locations of tags released east of 164°W was 56 +/- 4 cm s^{-1}, compared to 39 +/ 3 cm s^{-1} for tags released west of 164°W.

Movement models

The most parsimonious diffusion-taxis model estimated habitat preferences as a function of the 2D nonlinear interaction between depth and maximum tidal current velocity, and a nonlinear function of bottom temperature. This model also had the best predictive skill determined using RMSE (Table 2, Fig. 2). LOOCV showed that the selected diffusion-taxis model improved the prediction of held-out tag pop-up locations by 47%, bringing the RMS distance between observed and predicted pop-up locations down from 101.8 km using the diffusion-only model to 53.8 km using the diffusion-taxis model.

Visualizing marginal habitat preference smooths from the best-fit diffusion-taxis model revealed that, when depth and tidal current velocity were held at their average values, habitat preference was roughly flat until bottom temperatures (averaged to the 625 km^2 spatial scale) exceeded ~4.5°C (Fig. 2a). The slope of the habitat preference smooth became more steeply negative for temperatures > ~6°C, suggesting a lower preference for warmer bottom temperature habitats. Predicted habitat preferences relative to the nonlinear interaction between depth and maximum tidal current (with bottom temperature held at the average value) showed that BBRKC preferred habitat with either low maximum tidal currents and shallower depths, or high tidal currents and deeper depths (Fig. 2b). When tidal current velocity exceeded 48 cm s^{-1} (the median velocity), the range of depths where preference was greater than the 90th preference percentile was 69 m–104 m. Alternatively, when tidal currents were below the median, the range of depths where preference was greater than the 90th preference percentile was 33 m–45 m. As discussed above in *BBRKC movement patterns*, BBRKC preferentially moving into deeper habitat with greater exposure to tidal currents occurred largely within trawl closure areas in central and eastern Bristol Bay, whereas BBRKC preferentially moving into shallower habitat with less exposure to tidal currents occurred largely within northwestern Bristol Bay outside of trawl closure areas. Habitat preference

predictions over Bristol Bay showed that the areas with the highest preference extended in a band-like formation from the region within and around the RKCSA to the northwest into habitat falling outside the Bristol Bay management district (Fig. 3).

Projected BBRKC distributions and fishery overlap

Our analysis of spatial overlap between projected October BBRKC density and the directed BBRKC fishery (Figs. 4, 5; all distribution and overlap visualizations are provided in Appendix S1: Figs. 2-5) showed that diffusion-taxis model-based projections were consistently more similar to the fishery CPUE spatial distribution than those from the diffusion-only model. This was evidenced by a significantly higher degree of spatial overlap between diffusion-taxis model-based projections of density and fishing CPUE than overlap between the projections from the diffusion-only model and fishery CPUE for all years except 2007-2010 (Fig 5a). We found that centroids from diffusion-taxis model-based projections were significantly closer to directed fishery centroids in only 9 of 16 years, although centroids from diffusion-only model projections were never significantly closer to fishery centroids than those from the diffusion-taxis model.

The difference between overlap calculated from diffusion-taxis- and diffusion-only based projections (B_{DTM}–$B_{\mathrm{diff.\ only}}$) was well explained by October bottom temperatures in Bristol Bay: in years with cooler bottom temperature conditions, B_{DTM}–$B_{\mathrm{diff.\ only}}$ was near zero but the difference increased as bottom temperatures increased (Fig. 6, dev. expl. = 58.4%, edf = 1.9). Further analysis of the diffusion-taxis model-based projections showed a significant positive linear relationship between the longitude of the projected density centroid and the longitude of the centroid of fishery CPUE (Fig 7a, b, P = 0.001, R^2 = 0.55); however, a similar relationship was not found for latitude (Fig 7c, d). The time series of the longitudinal components of projected BBRKC density centroids (Fig. 7a) indicated that the autumn centroid of the stock shifted eastward between 2005 and 2010, remained near the eastern edge of the RKCSA between 2010 and 2014, and moved westward between 2015 and 2019. The longitudinal

454 component of the fishery CPUE showed a similar pattern, with a notable exception in 2017 when the
455 centroid of the fishery was further east than the projection centroid. In 2020, the directed fishery CPUE
456 centroid shifted eastward (no 2020 survey), and was similarly positioned in 2023 when the fishery re-
457 opened after two closed seasons. Projections estimated the position of the stock centroid to fall to the
458 northwest of the RKCSA in 2021 but predicted the centroid occurring within the RKCSA and further east
459 during 2022-2023 (Fig. 7a, c; Fig. 8a; no fishery during 2021/22 or 2022/23 seasons). In years when
460 October bottom temperatures were warmer, the position of the fishery centroid occurred farther west than
461 in cooler years, and the diffusion-taxis model projected that the centroid of the stock would be positioned
462 farther to the northwest relative to the position of the centroid during cooler years (Fig. 8a,b).

463 Discussion

464 We integrated the first *in situ* estimates of habitat preferences for mature male BBRKC during
465 late-spring to autumn migrations into a model of crab movement and used that model to make skillful
466 forecasts of BBRKC distributions from June to October. Our findings revealed that migrating crab
467 preferred regions of Bristol Bay where October bottom temperatures were, on average, $\lesssim 4.5$°C, and also
468 regions that were shallower, with lower tidal current exposure, or deeper, with higher tidal current
469 exposure. Predictions from the habitat preference model identified the regions with highest habitat
470 preference in October largely falling within the Red King Crab Savings Area (RKCSA), in addition to a
471 band of high preference habitat extending northwestward out of central Bristol Bay. Subsequent
472 movement-informed projections of BBRKC distribution over the June-October interval consistently
473 captured spatial variability in BBRKC fishery CPUE during the 2005-2023 period, in addition to
474 identifying regions where crab were expected to be, but where no fishing activity occurred. The westward
475 response of both the projected stock distribution and BBRKC fishery to warm bottom temperatures
476 suggests that future warming in Bristol Bay may lead to BBRKC distributional changes that lessen the
477 utility of the static RKCSA as an effective closure area.

Habitat preferences

Our findings showed that BBRKC habitat preferences were non-linearly related to October bottom temperatures and also related to the non-linear interaction of depths and maximum tidal current velocities across Bristol Bay. The habitat preference response of BBRKC to bottom temperatures displayed threshold-like behavior, with predicted habitat preference beginning to decline within the 4.5-6°C range. This result suggests that crab were unlikely to move into warmer bottom-temperature regions over the June-October interval that corresponded to shallow-water, nearshore habitats such as the Nearshore Bristol Bay Trawl Closure Area (NBBTCA). The use of spatiotemporally averaged temperatures from an oceanographic model as a covariate precludes the precise characterization of a bottom temperature threshold avoided by BBRKC. However, the downward turn in the habitat preference function that occurred in the 4.5-6°C range was consistent with laboratory experiments that evaluated Barents Sea RKC thermal preferences and found that mature males routinely preferred water temperatures < 4°C (Christiansen et al. 2015). While crab in this system have a strong preference for temperatures < 4°C, individuals also inhabited warmer temperatures in the 6-14°C range to a lesser extent, suggesting that RKC may trade off suitable bottom temperature conditions for other preferable environmental factors like prey availability when selecting habitats (Aune et al. 2022).

Tagged BBRKC displayed a clear preference for October habitats that were deeper than the habitat they occupied during June, with only 5 of 63 crabs moving to shallower habitat over the interval (caveated by our depth variable being averaged to the 625 km^2 grid cell). Additionally, October crab habitats were nearly uniformly found within the 50-100 m depth range that defines the middle shelf domain of Bristol Bay (Stabeno et al. 2010). Despite consistent seasonal movements into deeper water and into the middle shelf domain specifically, depth preferences were spatially variable. In central and eastern Bristol Bay (east of 164°W), crab preferred October habitats that were deeper, whereas crab in western Bristol Bay (west of 164°W) preferred shallower habitats.

A straightforward explanation for this spatial variability in preference may be related to a lack of available deeper habitat in the northwestern areas of the Bristol Bay management district, which is generally shallower than the preferred regions of central Bristol Bay, in addition to the presence of preferable bottom temperatures at shallower depths in this region. However, we found that depth preference was mediated by maximum tidal current velocities, a static prediction of water movement and the potential for interaction between currents and the benthos in the Bristol Bay management district (Laman et al. 2018). RKC mediate their movements based not only on preferable environmental conditions but also on food availability (Aune et al. 2022), and so the regions of high preference indicated by the interaction of depth and tidal current velocities may correspond to those regions where high-quality prey are available. Although observations of BBRKC prey distributions from the autumn are lacking, data from the NMFS EBS bottom trawl survey indicate that the middle shelf domain is dominated by benthic invertebrates that are primary contributors to BBRKC diets, including molluscs, echinoderms, and decapods (McLaughlin and Hebard 1959, Yeung and McConnaughey 2006). Future work characterizing the contributions of prey community dynamics to BBRKC habitat preferences, for instance by integrating spatiotemporally dynamic prey distribution maps (Reum et al. 2025) as covariates in habitat preference models, would shed further light on the spatially variable habitat preferences of BBRKC.

BBRKC seasonal projections and management implications

The hybrid SDM approach to seasonally projecting BBRKC distributions was effective in predicting the interannual spatial variability in fishery CPUE during the autumn, in addition to identifying regions of Bristol Bay where crab were likely to be abundant during the autumn, but where no fishing activity occurred. These higher density, no-fishing regions fell primarily along a band of high-preference habitat extending northwestward from central Bristol Bay. Our movement-informed projections did better at predicting the distribution of fishery CPUE than the projections made using diffusion-only models, indicating the importance of directional movement towards preferred habitat in shaping BBRKC seasonal

distribution. However, spatial overlap between fishery CPUE and projections using diffusion-taxis and diffusion-only models was similar in the 2007-2010 period when the distribution of the stock during the late spring was concentrated along the Alaska Peninsula (Appendix S1: Fig. S3).

Similar patterns in the distribution of BBRKC fishery catches along the Alaska Peninsula during these years have been associated with the presence of cooler bottom temperatures in the EBS (Zacher et al. 2018), and our diffusion-taxis model–based projections suggested that crab movement over the late spring–autumn interval away from the Alaska Peninsula was minimized due to the availability of preferable bottom temperature habitat near to late spring BBRKC habitat. Similar estimates of spatial overlap between the diffusion-taxis and diffusion-only model–based projections with fishery CPUE subsequently emerged due to the constraints placed on diffusive movement by the Alaska Peninsula: since the distribution of the stock during the late spring was concentrated in the nearshore, projected diffusive movement into central Bristol Bay was similar to projected movement based on diffusion and taxis, thereby resulting in similar levels of overlap between both projections and fishery CPUE.

The efficacy of our hybrid SDM in capturing the influence of bottom temperature on stock distribution was made clear by the similar longitudinal patterns exhibited by both projected BBRKC density and fishery CPUE in response to bottom temperatures. During years with warm October bottom temperatures, we found that both the distribution centroids of projected BBRKC density and fishery CPUE shifted further westward, a result that corroborates the finding that fishery CPUE is distributed farther southeast along the Alaska peninsula during cold years (Zacher et al. 2018). However, where our projections deviated from expectations was in showing that warmer bottom temperatures drove BBRKC stock distribution farther to the northwest than what was suggested by the distribution centroids of fishing CPUE alone. This deviation from what was seen in the distribution of fishing CPUE could indicate that the fishery was not as well-aligned with the distribution of the stock during autumns with warm bottom temperatures. A northward shift in the BBRKC stock has been noted previously in the context of BBRKC bycatch in flatfish fisheries and in the distribution of the stock during the late spring bottom trawl survey

(Ryznar and Litzow 2024), and the authors of that study conclude that this distribution shift suggests possible value in reconsidering the boundaries of the RKCSA. Our findings add to this discussion by presenting a novel perspective on BBRKC distribution shifts under warming based solely on fisheries-independent data. Our results suggest that under progressively warmer bottom temperature conditions in Bristol Bay, BBRKC stock distribution will continue tracking habitat preferences that are not constrained spatially to the RKCSA.

The spatial dynamism in habitat preferences that we have identified supports the consideration of dynamic spatial closures for BBRKC that may be more successful in optimizing across conflicting management goals than static closure areas (Hazen et al. 2018), and the delineation of these closure areas may benefit from the hybrid SDM approach we have advanced. However, the utility of the hybrid SDM approach in this context depends heavily on data availability, both of survey and tagging data, but also of environmental covariates; for example, bottom temperature layers that critically inform the dynamic aspects of the model. Indeed, the approach we have advanced could reasonably be applied in a true forecasting context, whereby future BBRKC distributions may be projected across seasons, when projections of dynamic environmental covariates become available. As it currently stands, the hybrid approach may be most useful in a scenario planning context. For example, autumn BBRKC distributions could be simulated under varying bottom temperature conditions to explore the impacts of bottom temperature on stock distribution. Future refinements to this method will benefit greatly from additional tagging data, and we advocate for the continued deployment of satellite tags not only on BBRKC but also on other crab species that are harvested in the EBS. Lastly, an important tradeoff in executing these projections during seasons when data are sparse is that projections cannot be easily validated; hence, why we compared our projections with CPUE observations from the directed BBRKC fishery. This consideration necessitates creative modeling solutions with careful execution, especially in the context of management decision-making.

Effective fisheries management requires accurate understanding of seasonal species distributions, yet many marine populations remain poorly observed outside limited survey windows, complicating efforts to predict interactions with fishing fleets. This knowledge gap presents a persistent obstacle when managing the spatial overlap between fisheries and vulnerable stocks remains a critical objective. Our study demonstrates that a hybrid species distribution modeling framework, which integrates movement data with habitat preferences, can successfully project seasonal shifts in the distribution of mature male Bristol Bay red king crab even in the absence of continuous observational data. By capturing the dynamic spatial responses of BBRKC to environmental variability, this approach offers a scalable solution to informing spatially adaptive management in data-limited contexts — a key advance in addressing one of the central challenges of managing mobile marine species under climate change.

Acknowledgements

We are grateful to the many scientists who have contributed to the NMFS EBS survey and BBRKC tagging programs over the years. We also thank Chris Siddon, Charles Perretti, and Devin Johnson for comments that strengthened earlier drafts. S. Hardison was supported by a postdoctoral fellowship from the Cooperative Institute for Climate, Ocean, and Ecosystem Studies (CICOES).

Figures

Table 1: Summary information from 2021-2023 tagging studies of mature male BBRKC.

Year	N tags	Avg. N days deployed	Avg. carapace length (mm)	SD carapace length (mm)	Tag deployment date range	Tag pop-up date range	Tag type
2021	13	128	147	10	Jun 2-Jun 12	Oct 12-Oct 13	All mrPAT
2022	13	126	148	14	May 30-Jun 22	Oct 12-Oct 13	All mrPAT
2023	37	131	146	14	May 29-Jun 18	Oct 13-Oct 15	31 mrPAT/6 MiniPAT

Table 2: Formulas for spline basis expansion that were used to estimate habitat preference models and crab taxis, where *te(...)* refers to the tensor product interaction smooth, *s(...)* the thin plate regression spline, and *k* the marginal basis dimension (with k - 1 degrees of freedom). The variable *velocity* is the predicted maximum tidal current velocity over the course of a year, *depth* is bottom depth, and *temp* is the average bottom temperature in the week of tag pop-up. "N pars." gives the number of estimated parameters in the movement model. Also included are movement model ΔAIC scores and root-mean squared error (RMSE) from the leave-one-out cross-validation analyses (in km). The best fitting model used in projection analyses is shown in bold.

Habitat preference formula	N pars.	ΔAIC	RMSE
te(depth, velocity, k = c(3,3)) + s(temp, k = 4)	**12**	**0.00**	**53.65**
te(velocity, temp, k = c(3,3)) + s(depth, k = 4)	12	7.89	56.34
te(depth, temp, k = c(3,3)) + s(velocity, k = 4)	12	44.95	58.77
s(velocity, k = 4) + s(temp, k = 4) + s(depth, k = 4)	10	48.19	60.83
velocity + temp + depth	4	102.85	71.71
diffusion only	1	219.18	101.79

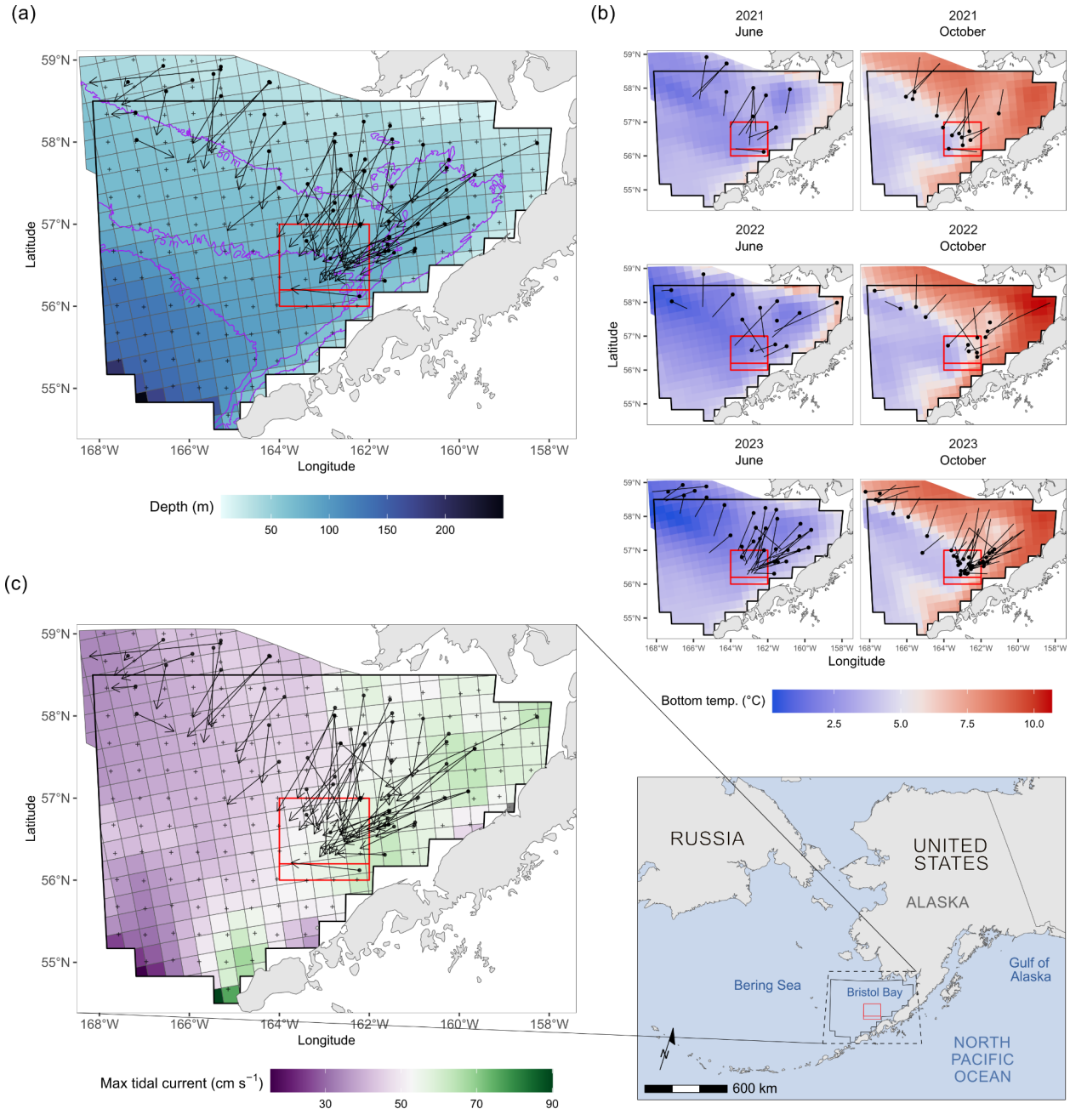

Figure 1. Environmental variables in Bristol Bay relative to June deployment locations and October pop-up locations of tagged BBRKC: (a) bathymetry with 50 m, 75 m, and 100 m depth contours, (b) MOM6 bottom temperatures during the second week of June (left) and October (right), and (c) maximum tidal currents. In maps (a) and (c), the locations of NMFS Eastern Bering Sea 2023 bottom trawl survey stations are marked with "+", and the start and end positions of crab tagged during 2021-2023 bottom trawl surveys are shown with black points and arrowheads, respectively. In map (b), the black points

indicate tag position and line segments indicate the observed movement path between tag deployment (left) and release (right). The bottom right map shows geographic context for the study area. In all maps, the black polygon represents the Bristol Bay RKC management district, and the red polygon is the Red King Crab Savings Area, within which falls the Red King Crab s-area (smaller rectangle).

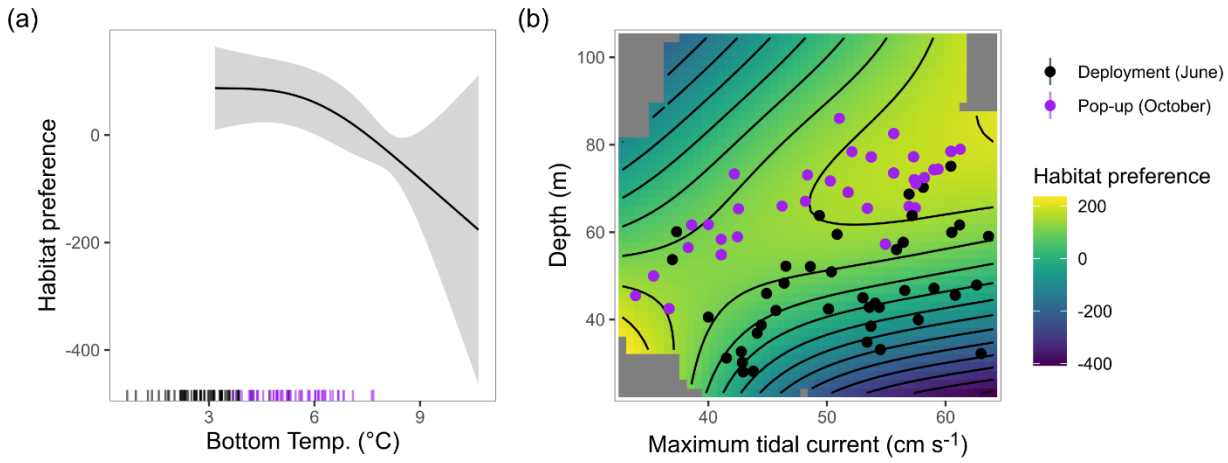

Figure 2. Marginal habitat preference smooths for bottom temperature (a) and the non-linear interaction of depth and maximum tidal currents (b). Vertical ticks in (a) and points in (b) show the values of environmental covariates at locations of tag deployment (black) and pop-up (purple). The region of (a) where the preference smooth for bottom temperature does not extend and the gray regions of (b) reflect October temperatures (during 2021-2023) and combinations of depth and tidal current, respectively, that did not occur in the Bristol Bay prediction grid.

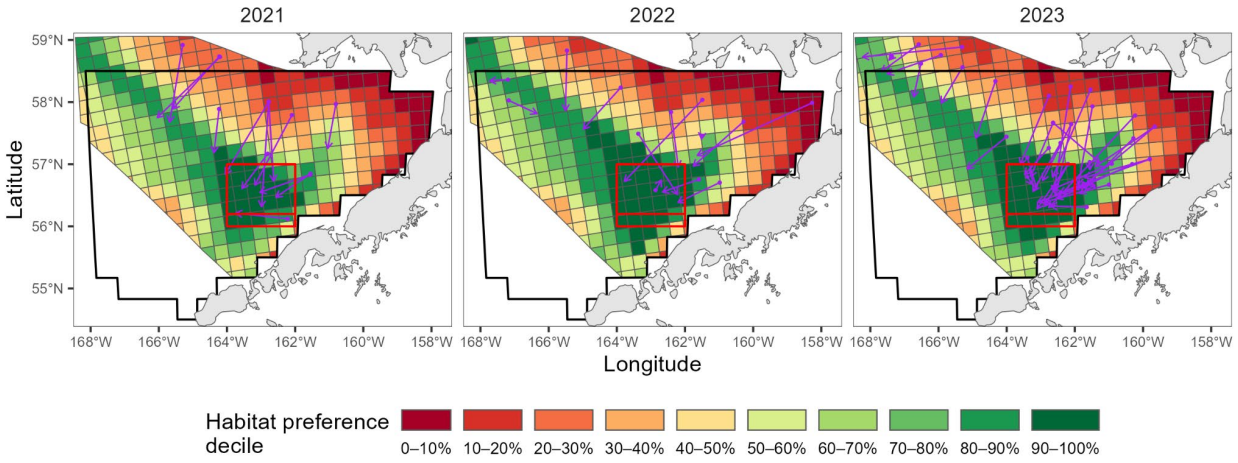

626

627 Figure 3. Habitat preference deciles predicted by the diffusion-taxis model for October 2021-2023. Purple
628 arrows are observed movement vectors. In all maps, the black polygon represents the Bristol Bay RKC
629 management district, and the red polygon is the Red King Crab Savings Area, within which falls the Red
630 King Crab Savings Sub-area (smaller rectangle).

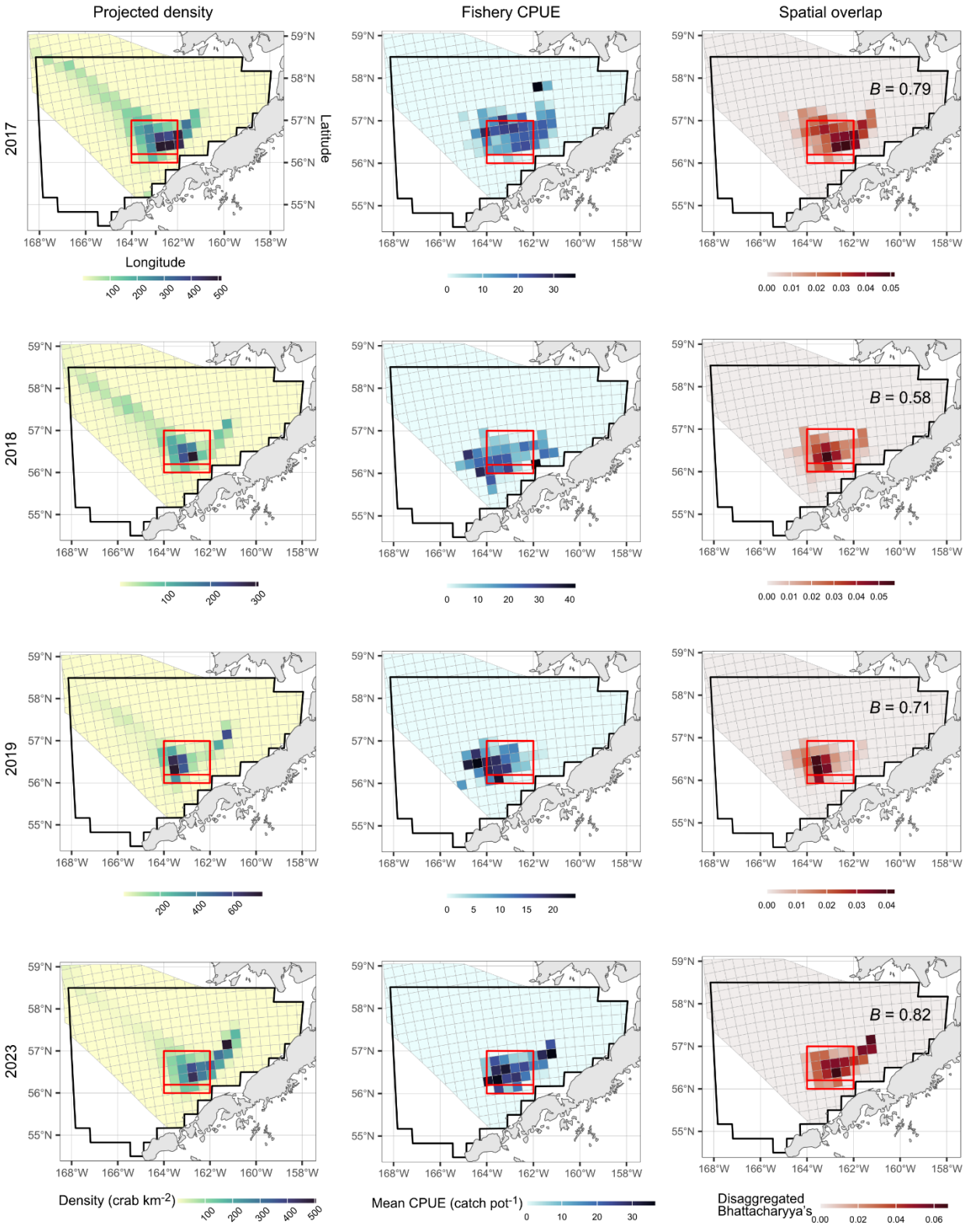
Projected density
Fishery CPUE
Spatial overlap
2017
2018
2019
2023
Latitude
Longitude
B = 0.79
B = 0.58
B = 0.71
B = 0.82
Density (crab km-2)
Mean CPUE (catch pot-1)
Disaggregated Bhattacharyya's

631

Figure 4. Projected October BBRKC density (left column), CPUE from the directed BBRKC fishery (middle), and Bhattacharyya's coefficient calculated from projected BBRKC density and CPUE in 2017-2023. Overlap could not be calculated for 2020-2022 due to the absence of an EBS bottom trawl survey in 2020 and fishery closures in 2021/22 and 2022/23. In all maps, the black polygon represents the Bristol Bay RKC management district, and the red polygon is the Red King Crab Savings Area, within which falls the Red King Crab Savings Sub-area (smaller rectangle).

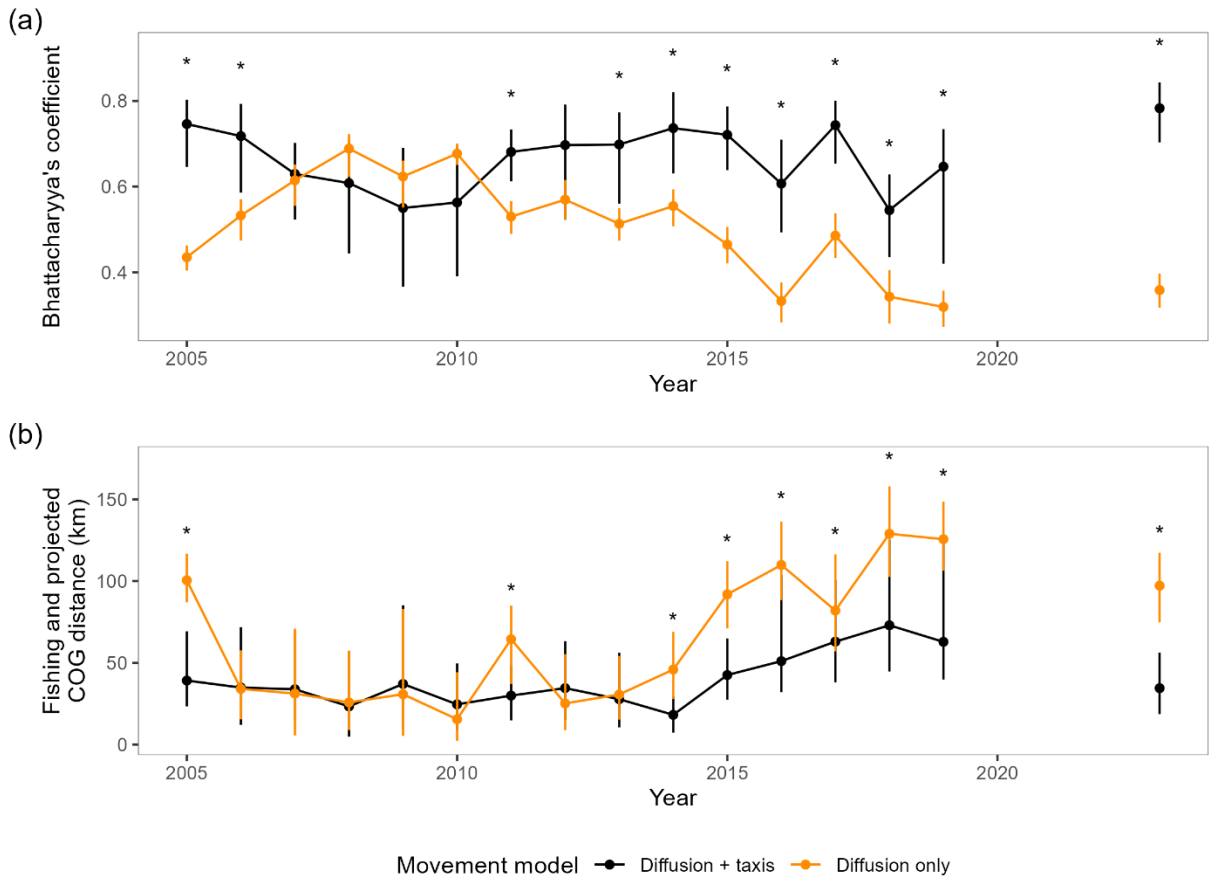

Figure 5. Spatial overlap time series between projected October BBRKC density and fishery catches (a) made using the diffusion-taxis model (black) or the diffusion-only model (orange). Distances between projected BBRKC density centroids made using the diffusion-taxis model (black) or diffusion-only model (orange) and BBRKC fishery centroids. Asterisks show significant differences between diffusion-taxis model and diffusion-only model results ($P < 0.05$).

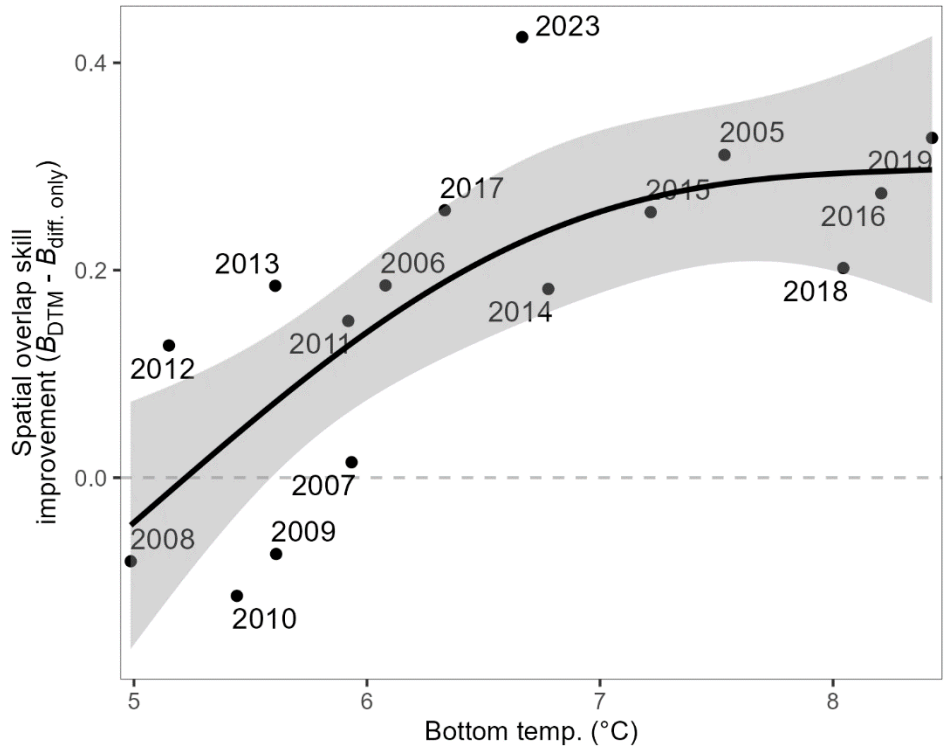

644

645 Figure 6. The improvement in predicting spatial overlap when estimating habitat preferences (y-axis;
646 measured as the difference in fishery overlap calculated using projections from the diffusion-taxis model
647 (B_{DTM}) and the diffusion-only model ($B_{diff. only}$)) and mean October bottom temperature in the Bristol Bay
648 management district.

649

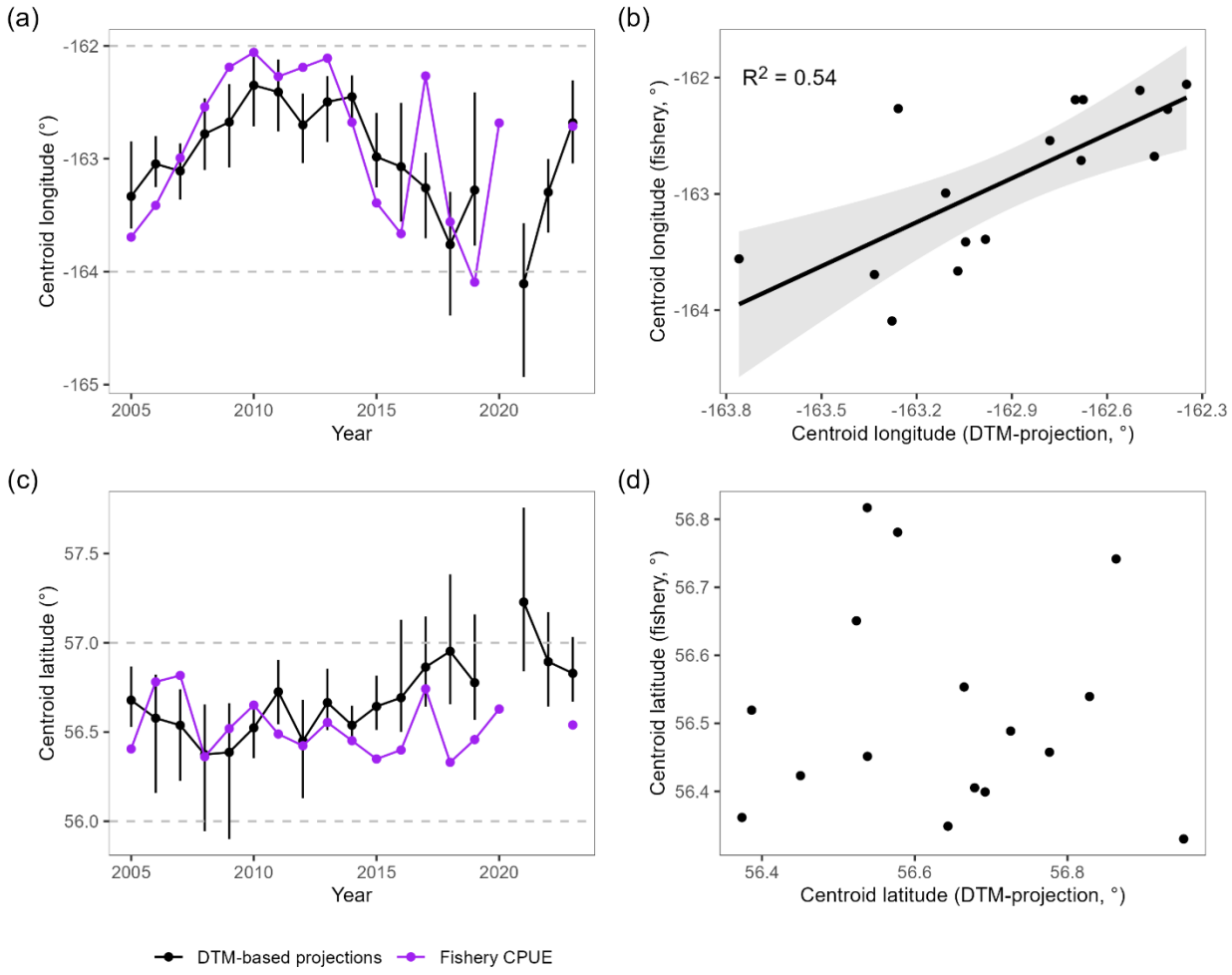

Figure 7. a) Longitudinal components of centroids for the directed BBRKC fishery (purple) and the diffusion-taxis model-based density projections (black, shown with 95% bootstrap confidence intervals), and b) the relationship between longitudes of fishery centroids and the annual mean longitude of projected density centroids from a bootstrap analysis. Similarly, the bottom row shows c) the time series of the latitudinal components of centroids and d) their linear relationship. In (a) and (c), gray dashed lines show the minimum and maximum longitude (a) and latitude (c) boundaries of the Red King Crab Savings Area.

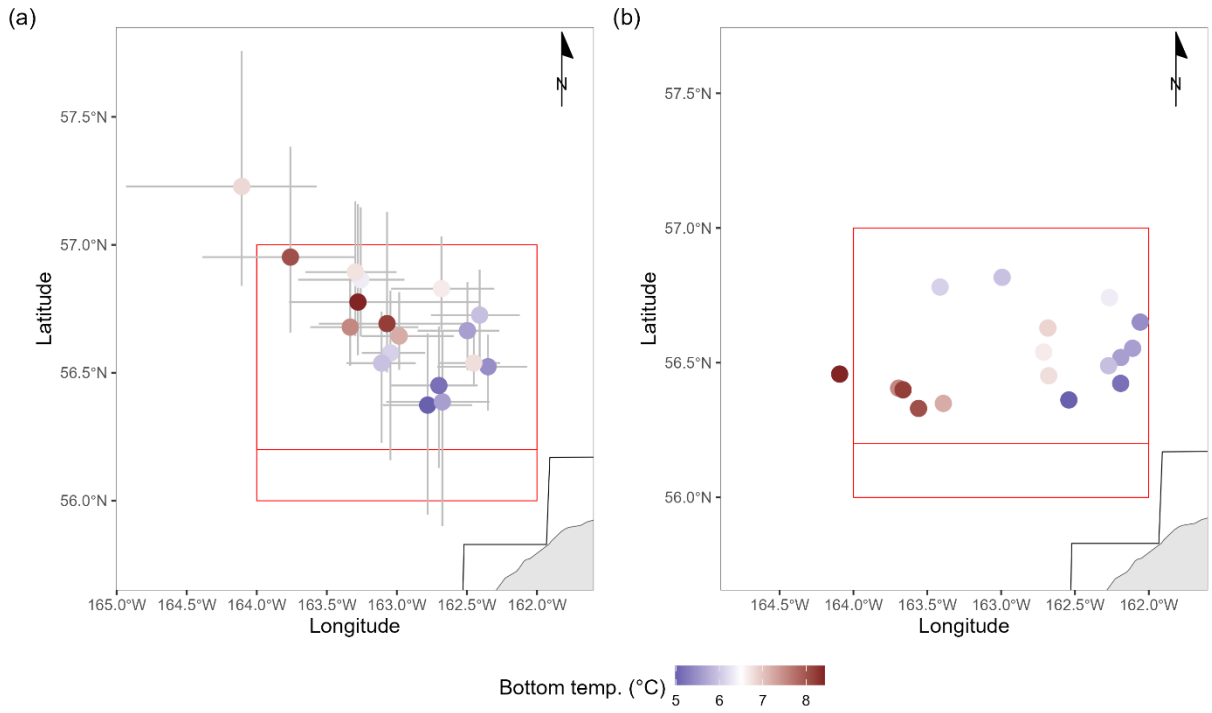

Figure 8. The annual centroids of projected BBRKC densities from the diffusion-taxis model (shown with 95% bootstrap confidence intervals) (a) and centroids of CPUE from the directed BBRKC fishery (b) shown with annual averages of October bottom temperatures over the prediction grid. The Red King Crab Savings Area is shown in red, with the smaller polygon referring to the Red King Crab Savings Sub-Area.

References

Aarts, Geert, et al. "Estimating space-use and habitat preference from wildlife telemetry data." *Ecography* 31.1 (2008): 140-160.

Akaike, Hirotugu. "Factor analysis and AIC." *Psychometrika* 52 (1987): 317-332.

Anderson, Sean C., et al. "sdmTMB: an R package for fast, flexible, and user-friendly generalized linear mixed effects models with spatial and spatiotemporal random fields." *BioRxiv* (2024): 2022-03.

Aune, Magnus, et al. "Space and habitat utilization of the red king crab (*Paralithodes camtschaticus*) in a newly invaded fjord in northern Norway." *Frontiers in Marine Science* 9 (2022): 762087.

Bhattacharyya, Anil. "On a measure of divergence between two statistical populations defined by their probability distribution." *Bulletin of the Calcutta Mathematical Society* 35 (1943): 99-110.

Carroll, Gemma, et al. "A review of methods for quantifying spatial predator–prey overlap." *Global Ecology and Biogeography* 28.11 (2019): 1561-1577.

Chilton, Elizabeth A., Robert J. Foy, and Claire E. Armistead. “Temperature effects on assessment of red king crab in Bristol Bay, Alaska.” (2010), 249-263. In G. H. Kruse, G. L. Eckert, R. J. Foy, R. N. Lipcius, B. Sainte-Marie, D. L. Stram, and D. Woodby (editors), Biology and Management of Exploited Crab Populations under Climate Change. Alaska Sea Grant Program Report AK-SG-10-01, University of Alaska, Fairbanks, AK.

Christiansen, Jørgen S., et al. "Thermal behaviour and the prospect spread of an invasive benthic top predator onto the Euro-Arctic shelves." *Diversity and Distributions* 21.9 (2015): 1004-1013.

Cressie, Noel, and Hsin-Cheng Huang. "Classes of nonseparable, spatio-temporal stationary covariance functions." *Journal of the American Statistical Association* 94.448 (1999): 1330-1339.

Dew, C. Braxton. "Red king crab mating success, sex ratio, spatial distribution, and abundance estimates as artifacts of survey timing in Bristol Bay, Alaska." *North American Journal of Fisheries Management* 28.5 (2008): 1618-1637.

Dew, C. Braxton, and Robert A. McConnaughey. "Did trawling on the brood stock contribute to the collapse of Alaska's king crab?" *Ecological Applications* 15.3 (2005): 919-941.

Drenkard, Elizabeth J., et al. “A regional physical-biogeochemical ocean model for marine resource applications in the Northeast Pacific (MOM6-COBALT-NEP10k v1.0).” *Geoscientific Model Development Discussions* 2024 (2024): 1-67.

Egbert, Gary D., and Svetlana Y. Erofeeva. "Efficient inverse modeling of barotropic ocean tides." *Journal of Atmospheric and Oceanic technology* 19.2 (2002): 183-204.

Fieberg, John, and Christopher O. Kochanny. "Quantifying home-range overlap: the importance of the utilization distribution." *The Journal of Wildlife Management* 69.4 (2005): 1346-1359.

Hazen, Elliott L., et al. "A dynamic ocean management tool to reduce bycatch and support sustainable fisheries." *Science Advances* 4.5 (2018): eaar3001.

Howard, Rebecca A., et al. "Projecting marine fish distributions during early life stages under future climate scenarios." *Fish and Fisheries* 25.4 (2024): 733-749.

Kristensen, Kasper. 2024b. RTMB: “R” Bindings for “TMB.” Available from https://CRAN.R708 project.org/package=RTMB.

Kruse, Gordon H., Jie Zheng, and Diana L. Stram. "Recovery of the Bristol Bay stock of red king crabs under a rebuilding plan." *ICES Journal of Marine Science* 67.9 (2010): 1866-1874.

Laman, Edward A., et al. "Using species distribution models to describe essential fish habitat in Alaska." *Canadian Journal of Fisheries and Aquatic Sciences* 75.8 (2018): 1230-1255.

Laman, E. A., J. L. Pirtle, J. Harris, M. C. Siple, C. N. Rooper, T. P. Hurst, and C. L. Conrath. *Advancing Model-Based Essential Fish Habitat Descriptions for North Pacific Species in the Bering Sea.*

U.S. Dept. of Commerce, NOAA Technical Memorandum NMFS-AFSC-459, Alaska Fisheries Science Center, 2022. https://doi.org/10.25923/y5gc-nk42

Lindgren, Finn, Håvard Rue, and Johan Lindström. "An explicit link between Gaussian fields and Gaussian Markov random fields: the stochastic partial differential equation approach." *Journal of the Royal Statistical Society Series B: Statistical Methodology* 73.4 (2011): 423-498.

Litzow, Michael A., et al. "Climate attribution time series track the evolution of human influence on North Pacific sea surface temperature." *Environmental Research Letters* 19.1 (2024): 014014.

Loher, Timothy, and David A. Armstrong. "Historical changes in the abundance and distribution of ovigerous red king crabs (*Paralithodes camtschaticus*) in Bristol Bay (Alaska), and potential relationship with bottom temperature." *Fisheries Oceanography* 14.4 (2005): 292-306.

Loher, T., et al. "2023 Early Spring Cooperative Pot Sampling (CPS1) for Bristol Bay District red king crab (*Paralithodes camtschaticus*)." (2024).

McLaughlin, Patsy A., and James F. Hebard. "Stomach contents of the Bering Sea king crab." U.S. Department of Interior, Fish and Wildlife Service, Special Scientific Report – Fisheries 291 (1959).

Markowitz, Emily H., et al. *Results of the 2022 Eastern and Northern Bering Sea Continental Shelf Bottom Trawl Survey of Groundfish and Invertebrate Fauna*. Alaska Fisheries Science Center (U.S.), NOAA Technical Memorandum NMFS-AFSC 469, 2023. doi:10.25923/rt50-th19.

Nault, Andrew J., et al. "Estimation of pop-up satellite archival tag initial surface position: applications for eastern Bering Sea crab research." *Animal Biotelemetry* 12.1 (2024): 7.

NPFMC. *Bristol Bay Red King Crab Information*. Discussion paper D1 BBRKC Info Paper, Apr. 2022a.

NPFMC. *Bristol Bay Red King Crab Expanded Information*. Discussion paper D2 BBRKC Expanded Discussion Paper, 21 Sep. 2022b.

NPFMC. *Considering a Closure to the Red King Crab Savings Area for All Gear Types.* Discussion paper C1 RKC Savings Area, 29 Nov. 2022c.

NPFMC. *Draft Environmental Assessment/Regulatory Impact Review for Proposed Amendment to the Fishery Management Plan for Groundfish of the Bering Sea/Aleutian Islands Management Area: Groundfish Area Closures within the Bristol Bay Red King Crab Stock Assessment Area*. 16 Jan. 2024a.

NPFMC. *Fishery Management Plan for Bering Sea/Aleutian Islands King and Tanner Crabs*. Oct. 2024b. https://www.npfmc.org/wp-content/PDFdocuments/fmp/Crab/CrabFMP.pdf

Palof, Katie. "Bristol Bay Red King Crab Stock Assessment 2024." *Bering Sea & Aleutian Islands Crab SAFE*. Sep. 2024.

Powell, G. C., and R. E. Reynolds. 1965. Movements of tagged king crabs, *Paralithodes camtschatica* (Tilesius), in the Kodiak Island-Lower Cook Inlet Region of Alaska, 1954-1963. Alaska Department of Fish and Game, Division of Commercial Fisheries, Informational Leaflet 55, Juneau.

R Core Team (2024). R: A language and environment for statistical computing. R Foundation for Statistical Computing, Vienna, Austria. URL https://www.R-project.org/.

Reum, Jonathan CP, et al. "Assessing benthos through predator stomach contents: spatiotemporal modeling of abundance and habitat use." *Ecography* (2025): e07723.

Ryznar, Emily R., and Michael A. Litzow. "Predicting the distribution of red king crab bycatch in Bering Sea flatfish trawl fisheries." *Fisheries Research* 279 (2024): 107158.

Ryznar, Emily R., and Michael A. Litzow. “Peering into the data-poor season: A fisheries-dependent distribution model to aid Bristol Bay red king crab management.” (2025). *in review*.

Seelanki, Vivek, et al. "Evaluation of a coupled ocean and sea-ice model (MOM6-NEP10k) over the Bering Sea and its sensitivity to turbulence decay scales." *EGUsphere* 2025 (2025): 1-40.

Stabeno, Phyllis, et al. "Factors influencing physical structure and lower trophic levels of the

eastern Bering Sea shelf in 2005: Sea ice, tides and winds." *Progress in Oceanography* 85.3-4 (2010): 180-196.

Stabeno, Phyllis J., and Shaun W. Bell. "Extreme conditions in the Bering Sea (2017–2018): Record-breaking low sea-ice extent." *Geophysical Research Letters* 46.15 (2019): 8952-8959.

Stone, Robert P., Charles E. O'Clair, and Thomas C. Shirley. "Seasonal migration and distribution of female red king crabs in a southeast Alaskan estuary." *Journal of Crustacean Biology* 12.4 (1992): 546-560.

Szuwalski, Cody, et al. "Climate change and the future productivity and distribution of crab in the Bering Sea." *ICES Journal of Marine Science* 78.2 (2021): 502-515.

Takeshita, K., H. Fujita, and S. Matsuura. "A note on population structure in the eastern Bering Sea adult red king crab, *Paralithodes camtschatica*." *Proceedings of the International Symposium on King and Tanner Crabs. Fairbanks: Alaska Sea Grant College Program, University of Alaska Fairbanks, AK-SG-90-04*. 1990.

Thorson, James T., et al. "Estimating fine-scale movement rates and habitat preferences using multiple data sources." *Fish and Fisheries* 22.6 (2021): 1359-1376.

Thorson, James, and Kasper Kristensen. *Spatio-temporal Models for Ecologists*. CRC Press, 2024.

Wallace, M. Marvin, Camile J. Pertuit, and Arthur R. Hvatum. "Contribution to the biology of the king Crab (*Paralithodes camtschatica* Tilesius)." Fish and Wildlife Service, United States Department of the Interior, Fishery Leaflet 340, 1949.

Wood, Simon N. "Generalized Additive Models: An Introduction with R. Chapman and Hall/CRC." *Texts Stat. Sci.* 67 (2006): 391.

Yeung, Cynthia, and Robert A. McConnaughey. "Community structure of eastern Bering Sea epibenthic invertebrates from summer bottom-trawl surveys 1982 to 2002." *Marine Ecology Progress Series* 318 (2006): 47-63.

Zacher, Leah Sloan, Gordon H. Kruse, and Sarah Mincks Hardy. "Autumn distribution of Bristol Bay red king crab using fishery logbooks." *Plos one* 13.7 (2018): e0201190.

Zacher, L. S., et al. *The 2024 Eastern Bering Sea Continental Shelf Trawl Survey: Results for Commercial Crab Species*. Alaska Fisheries Science Center, Resource Assessment and Conservation Engineering Division, NOAA Technical Memorandum NMFS-AFSC 491, 2024. doi:10.25923/q0fw-z324.

Zheng, Jie, and M. S. M. Siddeek. *Bristol Bay Red King Crab Stock Assessment in Fall 2018*. In *Stock Assessment and Fishery Evaluation Report for the 2018 Bering Sea–Aleutian Islands Crab Fishery*, North Pacific Fishery Management Council, 2018, pp. 1–140.

Appendix

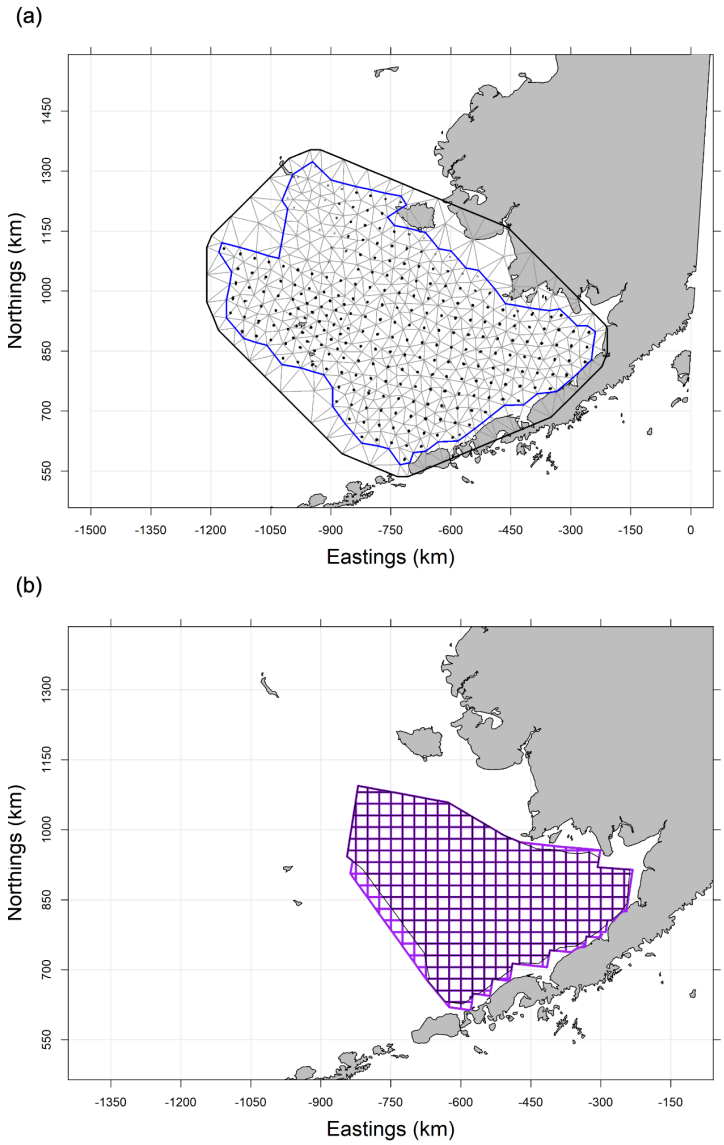

Figure S1. The SPDE mesh used in the estimation of the spatiotemporal model of red king crab density during the late spring, where points are locations of bottom trawl surveys during the 2005-2023 period (a). The prediction grid used to predict BBRKC densities from the spatiotemporal model and to project BBRKC densities into October (purple; b). Overlaid on the prediction grid is the grid used to build the adjacency matrix for fitting movement models (black; b).

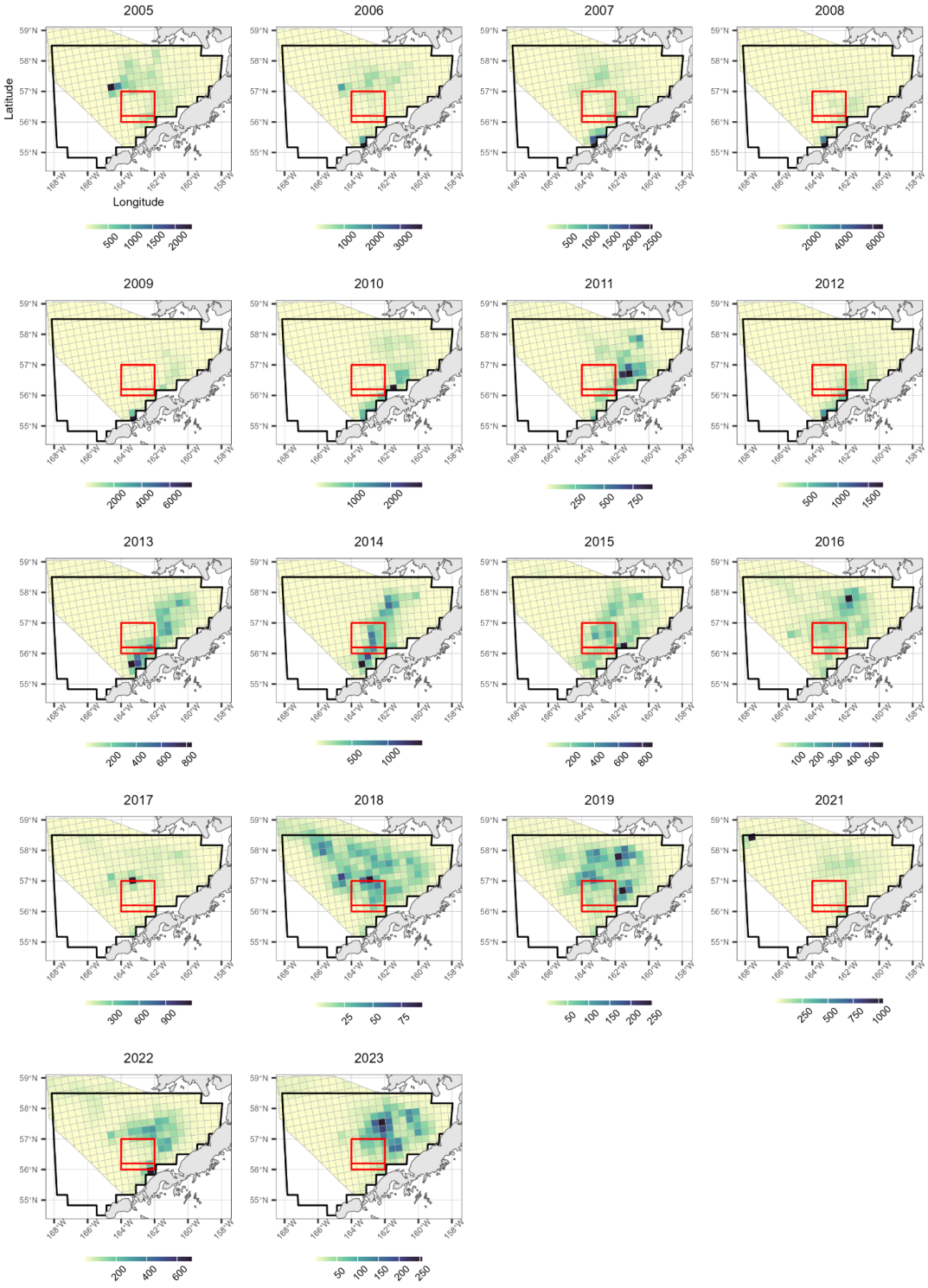

Figure S2. Year-to-year summertime distribution predictions from the spatiotemporal model. Colors reflect densities in crab km^{-2}. Note the differences in color scales between years.

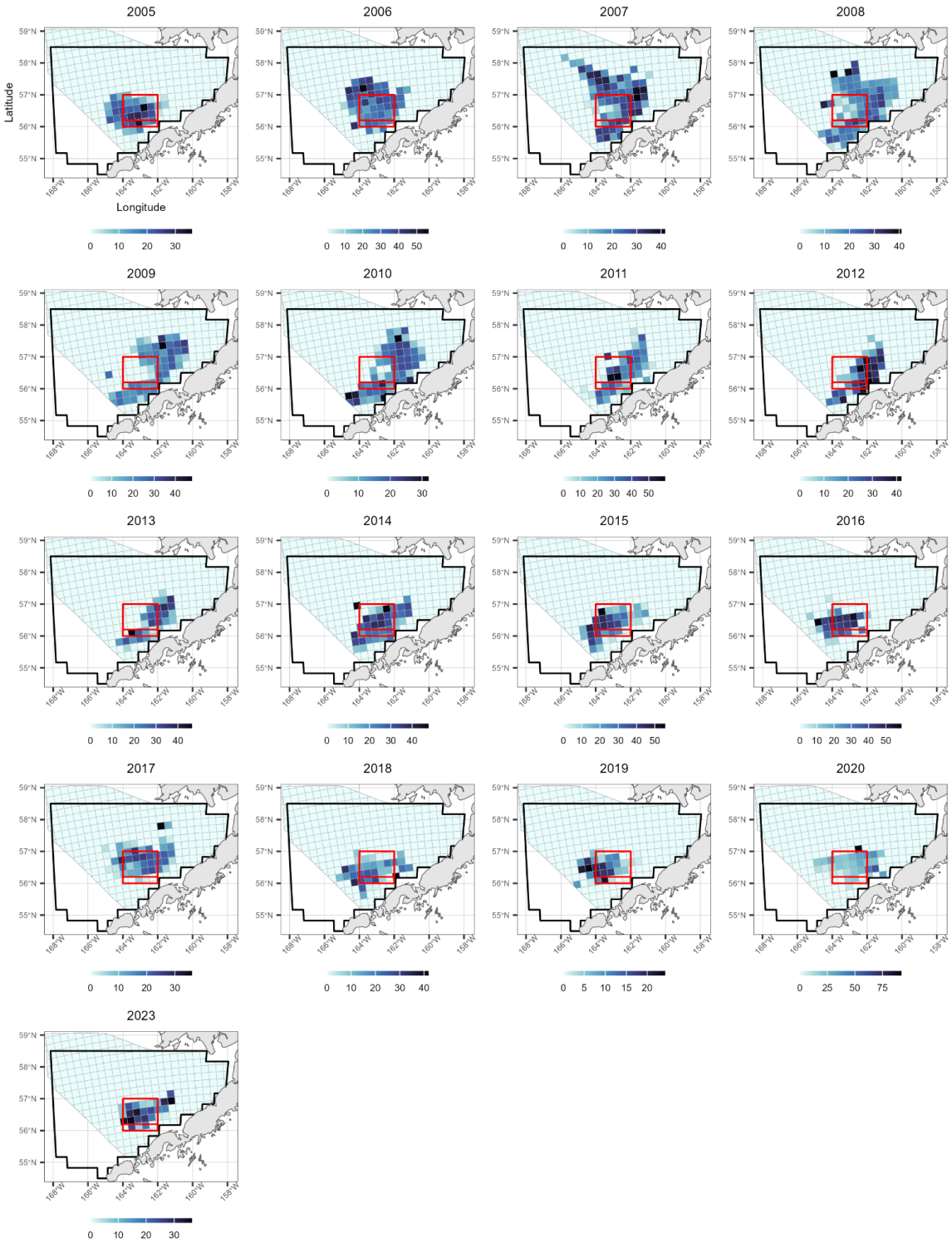

Figure S3. Year-to-year CPUE distributions from the BBRKC directed fishery. Colors reflect mean catch numbers pot^{-1}. Note the differences in color scales between years.

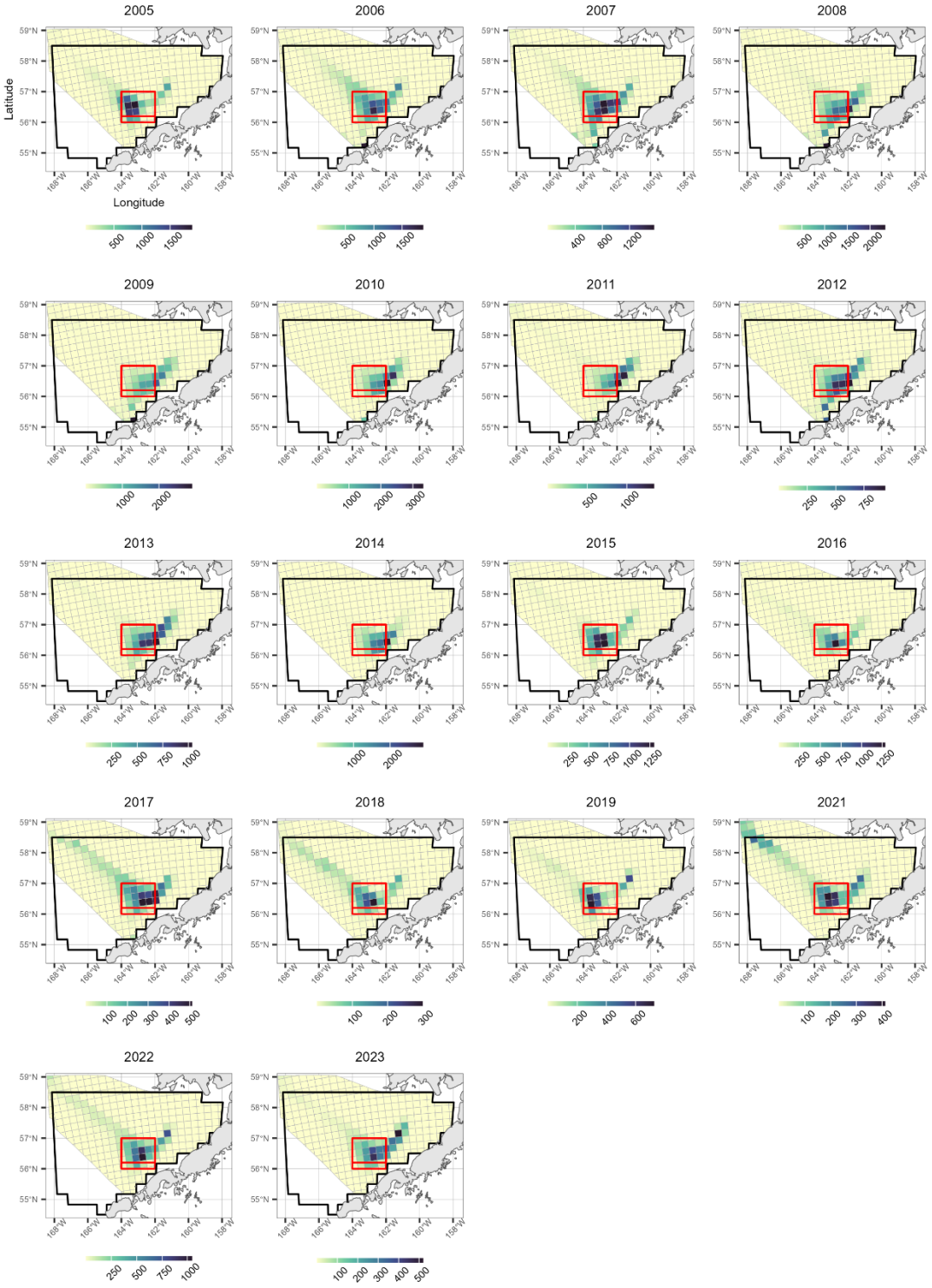

Figure S4. Year-to-year BBRKC October density projections using the diffusion-taxis model. Colors reflect densities in crab km^{-2}. Note the differences in color scales between years.

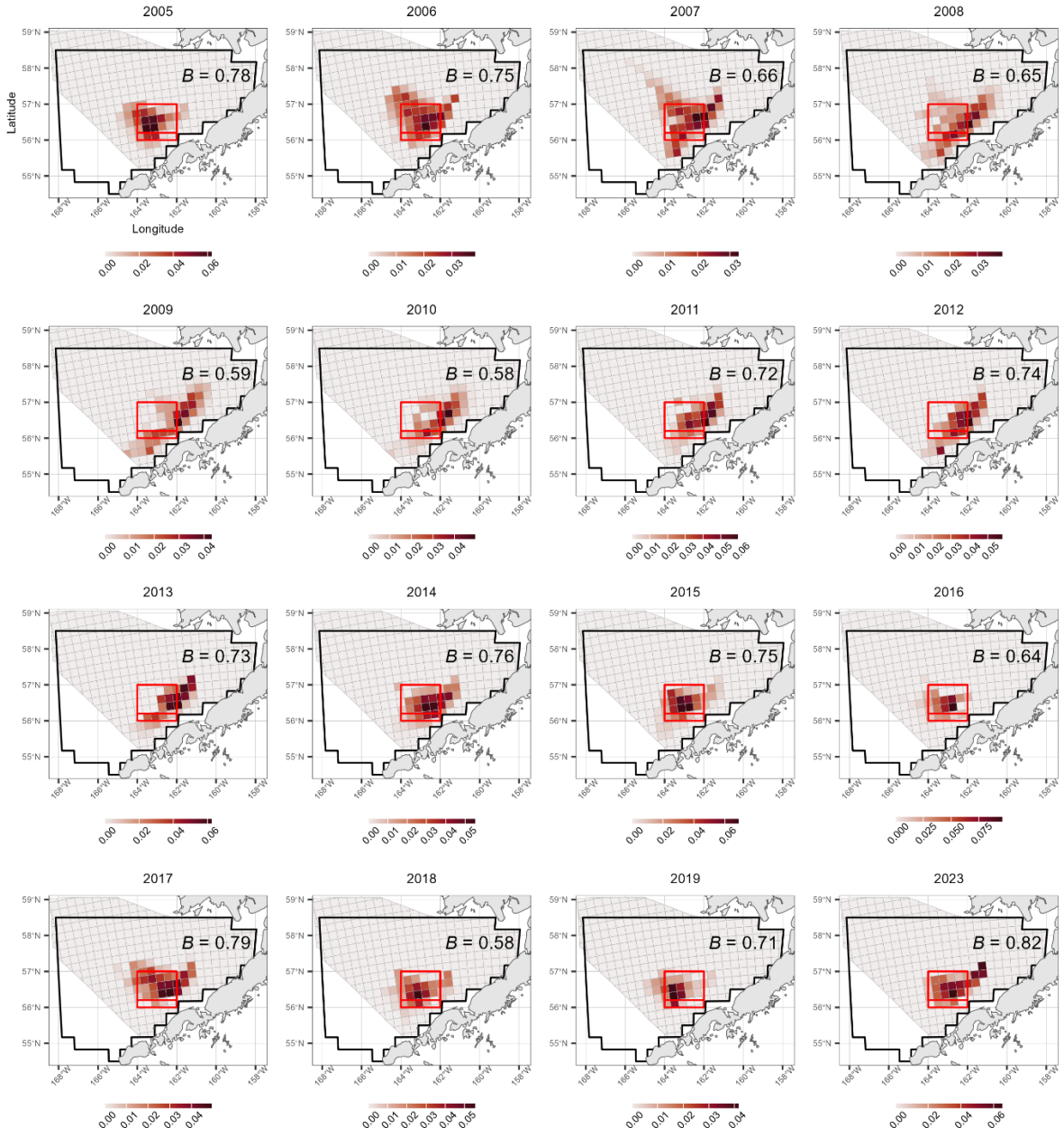

Figure S5. Year-to-year spatial overlap between projected BBRKC October densities and mean CPUE from the directed BBRKC fishery. Colors reflect the disaggregated Bhattacharyya overlap coefficient, i.e., the sum of overlap across cells is the Bhattachryya coefficient, *B*.